2-up-mix

NASA TECHNICAL NOTE

NASA TN D-7613

NASA TN D-7613

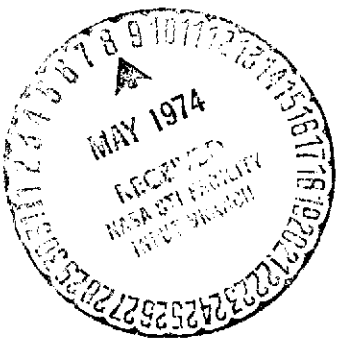

HIGH-TEMPERATURE MASS SPECTROMETRY - VAPORIZATION OF GROUP IVB METAL CARBIDES

by Carl A. Stearns and Fred J. Kohl

Lewis Research Center
Cleveland, Ohio 44135

NATIONAL AERONAUTICS AND SPACE ADMINISTRATION • WASHINGTON, D. C. • APRIL 1974

1. Report No.	2. Government Accession No.	3. Recipient's Catalog No.
NASA TN D-7613		

4. Title and Subtitle	5. Report Date
HIGH-TEMPERATURE MASS SPECTROMETRY - VAPORIZATION OF GROUP IVB METAL CARBIDES	APRIL 1974
	6. Performing Organization Code

7. Author(s)	8. Performing Organization Report No.
Carl A. Stearns and Fred J. Kohl	E-7510
	10. Work Unit No. 502-01

9. Performing Organization Name and Address	11. Contract or Grant No.
Lewis Research Center National Aeronautics and Space Administration Cleveland, Ohio 44135	
	13. Type of Report and Period Covered: Technical Note

12. Sponsoring Agency Name and Address	14. Sponsoring Agency Code
National Aeronautics and Space Administration Washington, D.C. 20546	

15. Supplementary Notes

16. Abstract

The high-temperature vaporization of the metal-carbon systems Ti-C, Zr-C, Hf-C, and Th-C was studied by the Knudsen effusion - mass spectrometric method. For each system the metal dicarbide and tetracarbide molecular species were identified in the gas phase. Relative ion currents of the carbides and metals were measured as a function of temperature. Second- and third-law methods were used to determine enthalpies for the reactions

$$M(g) + 2C(s) = MC_2(g)$$

$$M(g) + 4C(s) = MC_4(g)$$

Experimentally determined reaction enthalpies were combined with published thermodynamic data to obtain the following dissociation energies (in kJ mol^{-1}): D_0° (Ti-C_2) = 567±21, D_0° (Zr-C_2) = 575±24, D_0° (Hf-C_2) = 668±25, D_0° (Th-C_2) = 705±22, D_0° (C_2-Ti-C_2) = 1218±22, D_0° (C_2-Zr-C_2) = 1289±28, D_0° (C_2-Hf-C_2) = 1346±23, and D_0° (C_2-Th-C_2) = 1403±23. In addition, maximum values have been established for the dissociation energies of the metal monocarbide molecules TiC, ZrC, HfC, and ThC. Thermodynamic functions used in the calculations are discussed in terms of assumed molecular structures and electronic contributions to the partition functions. The trends shown by the dissociation energies of the carbides of Group IVB are compared with those of neighboring groups and discussed in relation to the corresponding oxides and chemical bonding. The high-temperature molecular beam inlet system and double-focusing mass spectrometer are described in detail.

17. Key Words (Suggested by Author(s))	18. Distribution Statement
High-temperature mass spectrometry; Knudsen effusion; Dissociation energies; Vaporization; Ti, Zr, Hf, and Th carbides; Ion counting	Unclassified - unlimited Category 06

19. Security Classif. (of this report)	20. Security Classif. (of this page)	21. No. of Pages	22. Price*
Unclassified	Unclassified	60	$3.75

* For sale by the National Technical Information Service, Springfield, Virginia 22151

HIGH-TEMPERATURE MASS SPECTROMETRY - VAPORIZATION OF GROUP IVB METAL CARBIDES*

by Carl A. Stearns and Fred J. Kohl

Lewis Research Center

SUMMARY

The high-temperature vaporization of the carbon-saturated carbides of titanium (Ti), zirconium (Zr), hafnium (Hf), and thorium (Th) was studied by the Knudsen effusion - mass spectrometric method. For each system the metal dicarbide and tetracarbide molecular species were identified in the gas phase. Relative ion currents of the carbides and metals were measured as a function of temperature. Second- and third-law methods were used to determine enthalpies for the reactions

$$M(g) + 2C(s) = MC_2(g)$$

$$M(g) + 4C(s) + MC_4(g)$$

Experimentally determined reaction enthalpies were combined with published thermodynamic data to obtain the following dissociation energies (in kJ mol^{-1}): D_0° ($Ti-C_2$) = 567±21, D_0° ($Zr-C_2$) = 575±24, D_0° ($Hf-C_2$) = 668±28, D_0° ($Th-C_2$) = 705±22, D_0° (C_2-Ti-C_2) = 1218±22, D_0° (C_2-Zr-C_2) = 1289±28, D_0° (C_2-Hf-C_2) = 1346±23, and D_0° (C_2-Th-C_2) = 1403±23. In addition, maximum values have been established for the dissociated energies of the metal monocarbide molecules TiC, ZrC, HfC, and ThC. Thermodynamic functions used in the calculations are discussed in terms of assumed molecular struc-

*An abbreviated account of this work was presented as a technical paper at the Nineteenth Annual Conference on Mass Spectrometry and Allied Topics, sponsored by the American Society of Mass Spectrometry and the American Society for Testing and Materials Committee E-14, Atlanta, Georgia, May 2-7, 1971, and printed as NASA TM X-67844, 1971.

tures and electronic contributions to the partition functions. The trends shown by the dissociation energies of the carbides of Group IVB are compared with those of neighboring groups and discussed in relation to the corresponding oxides and chemical bonding.

An appendix has been included to describe the high-temperature molecular beam inlet system and the double-focusing mass spectrometer used.

INTRODUCTION

Some of the transition metal carbides are included in the small group of materials which may be useful for structural applications at temperatures above 2500 K. Their melting points are not the primary limitation on the usefulness of these carbides. Thus, other factors such as brittleness and/or vaporization will determine the major mode of deterioration. The present study is concerned with the vaporization of the carbides of titanium (Ti), zirconium (Zr), hafnium (Hf), and thorium (Th). Some of our results for the titanium-carbon system have been reported in earlier publications (refs. 1 and 2). In this report, we reconsider the thermodynamics of the Ti-C molecules and compare them with the zirconium, hafnium, and thorium carbide molecules.

Vaporization studies of the Group IVB metal-carbon systems made prior to 1967 have been summarized in an excellent review by Storms (ref. 3). At that time it was generally believed that the vapor phase in equilibrium with the condensed carbides was composed of metal atoms and polymeric carbon species except for the thorium-carbon system. In that system, ThC_2 was shown to be the major gaseous thorium-containing species. Subsequent mass spectrometric vaporization studies of some transition metal-carbon (refs. 4 to 6) and rare-earth - carbon systems (refs. 7 to 10 (and refs. cited therein), 11 and 12) have established that the dicarbide (MC_2) and tetracarbide (MC_4) molecular species exist as stable molecules in the gas phase. The work reported herein is an extension of such studies to the Group IVB metal-carbon systems.

Vaporization studies of several rare-earth - carbon systems have demonstrated that the C_2^{-2} group behaves as a "pseudo-oxide" (refs. 7, and 10 to 14). Therefore, the existence of stable molecules of the type $M\text{-}C_2$ and $C_2\text{-}M\text{-}C_2$ was expected for the transition metals on the basis of the existence of the stable transition-metal monoxides and dioxides. The dissociation energies of the gaseous metal monocarbides of the electropositive transition elements have been estimated by an empirical procedure (ref. 15), but none have been observed experimentally. In contrast, for the noble metals platinum (Pt), iridium (Ir), rhodium (Rh), and ruthenium (Ru) the monocarbides are the major molecular species (refs. 16 and 17). A metal tricarbide molecule (MC_3) has been previously reported for only the lanthanum-carbon (La-C) system (ref. 10).

The existence of molecular titanium dicarbide was first reported in 1967 in reference 18. A subsequent study (refs. 1 and 2) established the dissociation energy of Ti-C_2 as 568±21 kJ mol^{-1}. This value was confirmed in another recent study (ref. 19).

The authors of reference 20 used a mass spectrometer and observed the $ZrC_2(g)$ molecule at high concentrations relative to the metal ($P_{Zr}/P_{ZrC_2} \cong 16$ at 2660 K over the ZrC-C-Ta system). They reported $\Delta G^{o}_{2660} = -109$ kJ mol^{-1} for the reaction

$$ZrC_2(g) = Zr(g) + C_2(g)$$

In 1970 the results of a mass spectrometric study of the vaporization of zirconium carbide from 2000 to 2900 K were reported (ref. 21). The authors do not report the observation of any molecular zirconium-carbon-containing species but do point out that no ZrC(g) was observed. We are unaware of the observation of any hafnium-carbon molecules prior to the present study.

References 22 to 24 show that the saturated vapors over thorium dicarbide contain atoms of Th and molecules of ThC_2 in approximately equal amounts. References 22 and 23 report the enthalpy for the reaction

$$ThC_2(s) = ThC_2(g)$$

as 828.9±14.6 kJ mol^{-1} and the standard heat of formation of $ThC_2(s)$ as $\Delta H^{o}_{f,\,298\ K} = -128.4 \pm 15.5$ kJ mol^{-1}.

In the present study, the Knudsen effusion method coupled with the use of a sophisticated double-focusing mass spectrometer was employed to study the vaporization of the respective metal carbide - carbon saturated phases. The primary objective of this research was to obtain experimental thermochemical data which could be used to specify the composition of the vapor phase for the metal carbides and to elucidate certain basic thermodynamic properties of simple gaseous molecules. These studies also help to establish the nature of high-temperature chemical reactions and to provide vapor pressure data which are of potential engineering value. In addition to their usefulness to materials engineers the data obtained can be beneficial in other disciplines. One example is the field of astrochemistry. Tsuji (ref. 25) has employed thermodynamic data for molecular carbide molecules to demonstrate that these species are important components in the atmospheres of carbon-rich cool stars.

DETAILS OF EXPERIMENT

In the course of our vaporization studies of various nitride, carbide, and oxide systems, numerous modifications have been incorporated into our high-temperature mass spectrometer facility as originally described in 1969 (ref. 26). Some of the details are contained in various reports (refs. 12, and 27 to 29), and some have never been published. Because the studies reported herein have had the advantages of most of the incorporated improvements, it is appropriate to describe the existing apparatus in some detail. A complete description of our Knudsen cell assembly and mass spectrometer is given in the appendix.

The procedure and experimental details employed to obtain data for the titanium-carbon system have been described in detail in references 1 and 2. Only those aspects pertinent to the comparisons made in this report are repeated herein.

For the experiments reported herein, an electron multiplier was used to measure ion currents, which were taken as a measure of ion intensity. The gain of the electron multiplier (electron output per ion input) for various ionic species was measured experimentally by ion-counting techniques with the SSR Instrument Company counting system (see appendix). Multiplier output current was measured by direct-current methods with a vibrating reed electrometer. Load resistors of 10^7, 10^8, and 10^9 ohms were used, and the integration time was between 10 and 20 seconds. Each ion intensity was measured at least five consecutive times, and the average value was calculated. The lowest detectable ion current was approximately 2×10^{-19} ampere at a signal-to-noise ratio of 3.2.

The carbides of titanium, zirconium, hafnium, and thorium were each prepared in either tungsten (W) or tantalum (Ta) Knudsen cells with graphite (Ultra Carbon Grade UFS) liners by heating mixtures of each metal powder with excess graphite powder (Ultra Carbon Grade UFS-4) under high vacuum. This preparation was done in situ in the mass spectrometer. At temperatures above 2000 K the metal and graphite reacted to form the carbon-saturated metal-carbide-condensed phases TiC + C, ZrC + C, HfC + C, and ThC_2 + C. In general, the carbide phase is somewhat substoichiometric and varies slightly in composition with temperature (ref. 3). Formation of the carbide phase in each case was verified by X-ray diffraction analysis of the samples.

PROCEDURE AND RESULTS

Vapor Species Identification and Appearance Potentials

The mass spectrum of each metal carbide - carbon system was examined in detail at mass-to-charge ratios m/e to about 300. In all cases the observed ions were

identified by mass-to-charge ratio and isotopic abundance. In addition to the metal ion (M^+) and various carbon polymer (C_1^+, C_2^+, C_3^+, C_4^+, C_5^+) ions, the dicarbide (MC_2^+) and tetracarbide (MC_4^+) ions were positively identified for each system. The metal monocarbide (MC^+) and tricarbide (MC_3^+) ions were identified at low intensity for the Zr, Hf, and Th systems but not for the Ti system. In the Hf experiment, Ta^+, TaC^+, and TaC_2^+ ions were observed, along with the analogous Hf- and C-containing species. These ions were assumed to result from the interaction of the graphite liner with the tantalum Knudsen cell. Shutter measurements were used to establish that all ion species of interest had neutral precursors originating from the Knudsen cell. None of the metals and carbide species were detected with the shutter closed.

The parent molecular species were identified by measurement of appearance potentials and ionization efficiency curves when ion intensities were sufficiently high. Measured values of the appearance potentials are listed in table 1. The low values of the appearance potentials for TiC_2^+, ZrC_2^+, ThC_2^+, TiC_4^+, and ThC_4^+ indicate that they are parent ions formed directly by electron impact of the respective molecules. It was assumed by analogy that the HfC_2^+, ZrC_4^+, and HfC_4^+ ions are also parent ion species even though their appearance potentials were not determined.

TABLE 1. - APPEARANCE POTENTIALS

Ion	Ti	Zr	Hf	Th
	Appearance potential, eV			
M^+	[a]6.82	[a]6.84	[a]7.0	[a]6.95
MC^+	(b)	(c)	(c)	8.0 ± 1.0
				[d]17.5 ± 1.0
MC_2^+	8.7 ± 0.5	7.5 ± 0.5	(c)	6.5 ± 0.3
MC_3^+	(b)	(c)	(c)	9.2 ± 1.0
MC_4^+	9.0 ± 1.0	(c)	(c)	10.0 ± 1.0

[a]Used as an internal standard for calibration of the electron energy scale (ref. 60).

[b]Ion not identified.

[c]Insufficient intensity for appearance potential measurement.

[d]Position of sharp upward break in ionization efficiency curve.

For the thorium system both ThC^+ and ThC_3^+ are probably parent ion species because their appearance potentials are low. The values estimated for the appearance potentials of ThC^+ and ThC_3^+ as fragments from ThC_2 and ThC_4, respectively, are

$$AP(ThC^+ \text{ fragment}) = AP(ThC_2^+) + D_0^\circ (C_2) = 6.5 \text{ eV} + 6.2 \text{ eV} = 12.7 \text{ eV}$$

and

$$AP(ThC_3^+ \text{ fragment}) = AP(ThC_4^+) + D_0^\circ (C_2) = 10.0 \text{ eV} + 6.2 \text{ eV} = 16.2 \text{ eV}$$

Because these estimates are considerably higher than the experimental values, we concluded that these species are parent ions. The ionization efficiency curve for ThC^+ had a sharp break at 17.5 ± 1.0 eV, which probably corresponds to the onset of a fragmentation reaction such as

$$ThC_2 + e^- = ThC^+ + C + 2e^-$$

The ThC^+ fraction which had an appearance potential of 8.0 ± 1.0 eV was estimated to be about 10 percent of the total ThC^+ ion current.

No definite assignment was made for the low-intensity ZrC^+, ZrC_3^+, HfC^+, or HfC_3^+, which may be either parent or fragment ions.

Ion Intensity Measurements

Ion currents were measured for the species M^+, MC_2^+, and MC_4^+ as a function of temperature for each of the metal-carbon systems. In addition, the intensities of MC^+ and MC_3^+ were measured at one or two temperatures for each system. The low temperature for each experiment is the temperature below which reliable measurements of the intensity could not be made for the least-abundant carbide species. The upper temperature of each experiment was set by experimental conditions involving the Knudsen cell. Both the tungsten and tantalum cells were partially carbided during the duration of the various experiments. Tungsten cells which had partially carbided tended to melt above 2875 K. Tantalum cells proved more useful, and the upper limit of 3100 K was caused by failure of the tungsten cell supports.

For at least one experiment on each metal-carbon system, a determination of the sensitivity constant relating pressure to ion intensity was made by calibration of the system using either gold (Ti experiment, refs. 1 and 2) or silver (Zr, Hf, and Th

experiments). For the silver calibration, a 0.005-millimeter-thick silver foil with a diameter equal to that of the interior of the Knudsen cell was placed over the sample in the Knudsen cell. The ion intensity of $^{107}Ag^+$ was measured at several temperatures below the melting point. Subsequently, the silver was melted and vaporized. From measurement of $^{107}Ag^+$ intensities and the known vapor pressure (ref. 30) of silver metal, the sensitivity constant was determined.

Titanium-carbon system. - Table 2 presents data for ion intensities of Ti^+, TiC_2^+,

TABLE 2. - ION INTENSITIES FOR THE TiC + C(s) SYSTEM

Temperature, K	$^{48}Ti^+$	$^{61}TiC^{+}$ [b]	$^{72}TiC_2^+$	$^{96}TiC_4^+$
	Multiplier anode current[a], A			
2585	2.10×10^{-7}	----------	1.78×10^{-9}	----------
2631	2.94	----------	2.81	----------
2644	4.48	----------	4.52	5.04×10^{-11}
2703	7.41	----------	8.96	1.42×10^{-10}
2774	1.18×10^{-6}	----------	1.94×10^{-8}	3.60
2741	8.88×10^{-7}	----------	1.25	1.92
2690	5.65	----------	6.40×10^{-9}	8.00×10^{-11}
2657	4.42	----------	4.40	6.40
2618	2.70	----------	2.16	2.52
2558	1.73	----------	1.20	----------
2518	1.05	----------	5.20×10^{-10}	----------
2551	1.52	----------	9.28	----------
2608	2.62	----------	2.18×10^{-9}	----------
2669	4.74	----------	4.60	5.60×10^{-11}
2725	7.25	----------	9.60	1.44×10^{-10}
2757	9.04	----------	1.25×10^{-8}	2.04
2790	1.25×10^{-6}	----------	2.16	4.40
[c]2580	1.44	$<6.0 \times 10^{-12}$	----------	----------

[a]Measurements were made using 20-eV electrons at 150-μA anode current. Sample was contained in a graphite liner in a tungsten cell. Gold pressure calibration was made. (Refs. 1 and 2.)

[b]The major TiC^+ isotopic peak at m/e = 60 could not be measured because of a large Ni^+ impurity.

[c]Separate experiment.

TABLE 3. - ION INTENSITIES MEASURED FOR THE ZrC + C(s) SYSTEM

Temperature, K	$^{90}Zr^+$	$^{102}ZrC^+$	$^{114}ZrC_2^+$	$^{126}ZrC_3^+$	$^{138}ZrC_4^+$
	Multiplier anode current[a], A				
Experiment A[b]					
2775	6.40×10^{-10}	----------	---	----------	5.52×10^{-12}
2773	4.40	----------	1.44×10^{-10}	----------	3.36
2944	3.32×10^{-9}	----------	1.80×10^{-9}	----------	1.56×10^{-10}
2802	4.80×10^{-10}	----------	2.09×10^{-10}	----------	9.12×10^{-12}
2911	1.80×10^{-9}	----------	1.27×10^{-9}	----------	7.60×10^{-11}
2967	3.36	1.20×10^{-10}	2.11	1.18×10^{-10}	2.04×10^{-10}
2824	4.96×10^{-10}	----------	2.59×10^{-10}	----------	9.60×10^{-12}
Experiment B[c]					
2839	5.60×10^{-10}	----------	2.28×10^{-10}	----------	9.12×10^{-12}
2867	9.12	----------	4.40	----------	1.56×10^{-11}
2805	3.92	----------	1.44	----------	3.20×10^{-12}
2737	1.54	----------	4.40×10^{-11}	----------	----------
2688	7.60×10^{-11}	----------	1.99	----------	----------
2670	6.80	----------	1.32	----------	----------
2701	1.27×10^{-10}	----------	3.20	----------	----------
2767	2.52	----------	7.60	----------	----------
2824	6.24	----------	2.64×10^{-10}	----------	1.08×10^{-11}
2862	8.00	----------	4.80	----------	1.68
2918	1.68×10^{-9}	----------	8.64	----------	5.44
Experiment C[b]					
2922	1.32×10^{-9}	----------	6.08×10^{-10}	----------	2.28×10^{-11}
2836	3.20×10^{-10}	----------	1.49	----------	5.52×10^{-12}
2719	5.44×10^{-11}	----------	1.27×10^{-11}	----------	----------
2785	1.56×10^{-10}	----------	5.44	----------	----------
2864	4.00	----------	2.04×10^{-10}	----------	7.20×10^{-12}
2925	7.68	----------	4.48	----------	2.11×10^{-11}
2988	1.54×10^{-9}	----------	8.40	----------	6.24
2957	1.25	----------	6.80	----------	4.40
3003	1.92	8.24×10^{-11}	1.10×10^{-9}	4.80×10^{-11}	7.20
2722	3.60×10^{-11}	----------	9.12×10^{-12}	----------	----------
2904	5.60×10^{-10}	----------	2.69×10^{-10}	----------	1.15×10^{-11}
2947	8.40	----------	5.52×10^{-10}	----------	2.14
2875	3.76	----------	1.90	----------	----------
2842	2.50	----------	1.18	----------	----------
2681	1.80×10^{-11}	----------	3.44×10^{-12}	----------	----------
2705	2.28	----------	5.20	----------	----------
2743	5.36	----------	1.32×10^{-11}	----------	----------
2747	6.88	----------	1.80	----------	----------
2806	1.32×10^{-10}	----------	3.84	----------	----------
2960	1.18×10^{-9}	----------	5.68×10^{-10}	----------	----------

[a]Measurements were made using 40-eV electrons at 200-μA anode current for each experiment. Sample was contained in a graphite liner in a tantalum cell.

[b]No pressure calibration was made.

[c]Silver pressure calibration was made.

TABLE 4. - ION INTENSITIES MEASURED FOR THE HfC + C(s) SYSTEM

Temperature, K	$^{178}Hf^+$	$^{190}HfC^+$	$^{203}HfC_2^+$	$^{216}HfC_3^+$	$^{228}HfC_4^+$
	Multiplier anode current[a], A				
2952	1.15×10^{-10}	----------	3.20×10^{-10}	----------	----------
3013	1.54	5.39×10^{-12}	4.87	4.01×10^{-12}	1.20×10^{-11}
3066	1.82	1.05×10^{-11}	6.48	4.09	1.63
3030	4.95×10^{-11}	----------	9.74×10^{-12}	----------	----------

[a]Measurements were made using 40-eV electrons at 200-μA anode current. Sample was contained in a graphite liner in a tantalum cell. Silver pressure calibration was made.

TABLE 5. - ION INTENSITIES MEASURED FOR THE ThC_2 + C(s) SYSTEM

Temperature, K	$^{232}Th^+$	$^{244}ThC^+$	$^{256}ThC_2^+$	$^{268}ThC_3^+$	$^{280}ThC_4^+$
	Multiplier anode current[a], A				
2742	3.20×10^{-10}	----------	4.08×10^{-10}	----------	5.44×10^{-11}
2686	1.54	----------	1.80	----------	1.68
2711	1.94	----------	2.30	----------	2.45
2747	2.59	----------	3.60	----------	4.72
2773	4.40	----------	5.68	----------	7.04
2837	6.80	----------	9.44	----------	1.63×10^{-10}
2855	8.40	----------	1.42×10^{-9}	----------	2.26
2890	1.34×10^{-9}	[b]5.60×10^{-11}	1.92	3.60×10^{-11}	3.92
2906	1.56	----------	2.40	----------	4.56
2804	5.28×10^{-10}	----------	7.84×10^{-10}	----------	1.22
[c]2963	2.45×10^{-9}	9.68×10^{-12}	----------	----------	----------

[a]Measurements were made using 22-eV electrons at 100-μA anode current. Sample was contained in a graphite liner in a tantalum cell. Silver pressure calibration was made.

[b]Estimate that parent ThC^+ is 10 percent of total ThC^+ intensity, 5.60×10^{-12} A.

[c]Separate experiment using 16-eV electrons at 50-μA anode current to record mostly parent ThC^+.

and TiC_4^+ which were measured at 17 temperatures between 2518 and 2790 K. Data points were taken for both increasing and decreasing sequences of temperature. Ion intensities at any particular temperature were found to remain constant for a period of at least 20 hours (refs. 1 and 2). This demonstrated the time independence of the experment.

Zirconium-carbon system. - Three separate experiments were performed on Zr-C, covering the temperature range 2670 to 3003 K and yielding data at 38 temperatures. The ion currents for Zr^+, ZrC^+, ZrC_2^+, ZrC_3^+, and ZrC_4^+ are listed in table 3.

Hafnium-carbon system. - Ion intensities of Hf^+, HfC^+, HfC_2^+, HfC_3^+, and HfC_4^+ were measured at four temperatures between 2952 and 3066 K. These intensities are given in table 4.

Thorium-carbon system. - To measure the intensities of Th^+, ThC^+, ThC_2^+, ThC_3^+, and ThC_4^+, an experiment covering 10 temperatures between 2686 and 2906 K was carried out. The ion intensities are listed in table 5.

CALCULATIONS

Pressures

The currents I_i, in amperes, measured at the anode of the electron multiplier for individual species i were converted to corresponding partial pressures P_i, in N/m^2, at temperature T, in kelvins, by the relation

$$P_i = \frac{kI_iTE_i}{\sigma_i \gamma_i n_i}$$

where k, in $N\ m^{-2}A^{-1}K^{-1}$, is the sensitivity constant determined by the silver or gold calibration; σ_i is the relative maximum ionization cross section; γ_i, in electrons per incident ion, is the multiplier gain; n_i is the fractional isotopic abundance of the species i for the isotope measured; and E_i is an experimentally determined dimensionless factor to correct ion intensities measured at a particular ionizing electron energy to the maximum of the ionization efficiency curve (i.e., ratio of ion intensity at the maximum of the ionization efficiency curve to intensity at the electron energy used in the measurements).

Ionization cross sections for atoms were taken from Mann (ref. 31), and the cross sections for the MC_2 and MC_4 were obtained by summing the atomic cross sections for the metal and two and four carbon atoms, respectively. The values of k, σ, γ, n, and E are given for each experiment where pressures were determined in table 6.

TABLE 6. - MEASURED AND ESTIMATED PARAMETERS FOR VARIOUS IONS

Ion	Ionization cross section, σ	Multiplier gain[a], γ	Intensity correction factor[b], E	Isotopic abundance, n
System: TiC + C; $k = 1.16\times10^{11}$ N $m^{-2}A^{-1}K^{-1}$				
$^{197}Au^+$	6.46	8.27×10^6	1.42	1.0000
$^{48}Ti^+$	5.97	1.21×10^7	1.00	.7394
$^{61}TiC^+$	7.70	[c](1.21×10^7)	(1.00)	.0627
$^{72}TiC_2^+$	9.43	1.70×10^7	1.16	.7232
$^{96}TiC_4^+$	12.89	1.71	(1.16)	.7101
System: ZrC + C; experiment B; $k = 1.38\times10^{11}$ N $m^{-2}A^{-1}K^{-1}$				
$^{107}Ag^+$	5.44	6.64×10^6	1.00	0.5182
$^{90}Zr^+$	7.90	7.77	1.00	.5146
$^{102}ZrC^+$	9.63	(7.77×10^6)	(1.00)	.5089
$^{114}ZrC_2^+$	11.36	8.28×10^6	(1.00)	.5032
$^{138}ZrC_4^+$	14.82	(8.28×10^6)	(1.00)	.4921
System: HfC + C; $k = 3.75\times10^{11}$ N $m^{-2}A^{-1}K^{-1}$				
$^{107}Ag^+$	5.44	7.00×10^6	1.00	0.5182
$^{178}Hf^+$	7.76	7.35	1.00	.2714
$^{190}HfC^+$	9.49	(7.35×10^6)	(1.00)	.2704
$^{203}HfC_2^+$	11.22	(7.35×10^6)	(1.00)	.1404
$^{228}HfC_4^+$	14.68	(7.35×10^6)	(1.00)	.3430
System: ThC_2 + C; $k = 7.50\times10^{11}$ N $m^{-2}A^{-1}K^{-1}$				
$^{107}Ag^+$	5.44	7.00×10^6	1.00	0.5182
$^{232}Th^+$	12.91	6.49	[d]1.00	1.0000
$^{244}ThC^+$	14.64	(6.50×10^6)	(1.00)	.9889
$^{256}ThC_2^+$	16.37	6.51×10^6	[d]1.21	.9779
$^{280}ThC_4^+$	19.83	7.29	[d]1.76	.9563

[a]Multiplier gain at 256 V/stage for 17-stage multiplier.

[b]For 37-eV electrons.

[c]Values in parentheses are estimated.

[d]For 20-eV electrons.

TABLE 7. - PARTIAL PRESSURES OF Ti(g), TiC_2(g), AND TiC_4(g) OVER TiC + C(s)

Temperature, K	Ti	TiC_2	TiC_4
	Pressure, N m^{-2}		
2585	1.18	5.30×10^{-3}	----------
2631	1.68	8.52	----------
2644	2.57	1.38×10^{-2}	1.13×10^{-4}
2703	4.35	2.80	3.27
2774	7.08	6.20	8.53
2741	5.29	3.95	4.50
2690	3.30	1.99	1.84
2657	2.55	1.35	1.45
2618	1.54	6.53×10^{-3}	5.63×10^{-5}
2558	.961	3.55	----------
2518	.573	1.51	----------
2551	.842	2.74	----------
2608	1.49	6.58	----------
2669	2.75	1.42×10^{-2}	1.28×10^{-4}
2725	4.29	3.02	3.35
2757	5.41	3.97	4.80
2790	7.56	6.95	1.05×10^{-3}

TABLE 8. - PARTIAL PRESSURES OF Zr(g), ZrC_2(g), AND ZrC_4(g) OVER ZrC + C(s)

Temperature, K	Zr	ZrC_2	ZrC_4
	Pressure, N m^{-2}		
2839	6.95×10^{-3}	1.89×10^{-3}	5.92×10^{-5}
2867	1.14×10^{-2}	3.68	1.02×10^{-4}
2805	4.80×10^{-3}	1.18	2.05×10^{-5}
2737	1.84	3.51×10^{-4}	----------
2688	8.92×10^{-4}	1.56	----------
2670	7.93	1.03	----------
2701	1.50×10^{-3}	2.52	----------
2767	3.05	6.13	----------
2824	7.70	2.17×10^{-3}	6.97×10^{-5}
2862	1.00×10^{-2}	4.01	1.10×10^{-4}
2918	2.14	7.35	3.63

TABLE 9. - PARTIAL PRESSURES OF Hf(g), HfC_2(g), AND HfC_4(g) OVER HfC + C(s)

Temperature, K	Hf	HfC_2	HfC_4
	Pressure, N m^{-2}		
2952	8.22×10^{-3}	3.06×10^{-3}	----------
3013	1.12×10^{-2}	4.75	3.66×10^{-4}
3066	1.35	6.43	5.06
[a]3030	----------	----------	----------

[a]Position of cell was changed; therefore, no pressures are calculated.

TABLE 10. - PARTIAL PRESSURES OF Th(g), ThC_2(g), AND ThC_4(g) OVER ThC_2 + C(s)

Temperature, K	Th	ThC_2	ThC_4
	Pressure, N m^{-2}		
2742	7.85×10^{-3}	9.74×10^{-3}	1.42×10^{-3}
2686	3.70	4.21	4.31×10^{-4}
2711	4.71	5.43	6.34
2747	6.37	8.61	1.24×10^{-3}
2773	1.09×10^{-2}	1.37×10^{-2}	1.86
2837	1.73	2.33	4.42
2855	2.15	3.53	6.16
2890	3.47	4.83	1.08×10^{-2}
2906	4.06	6.07	1.27
2804	1.33	1.91	3.27×10^{-3}

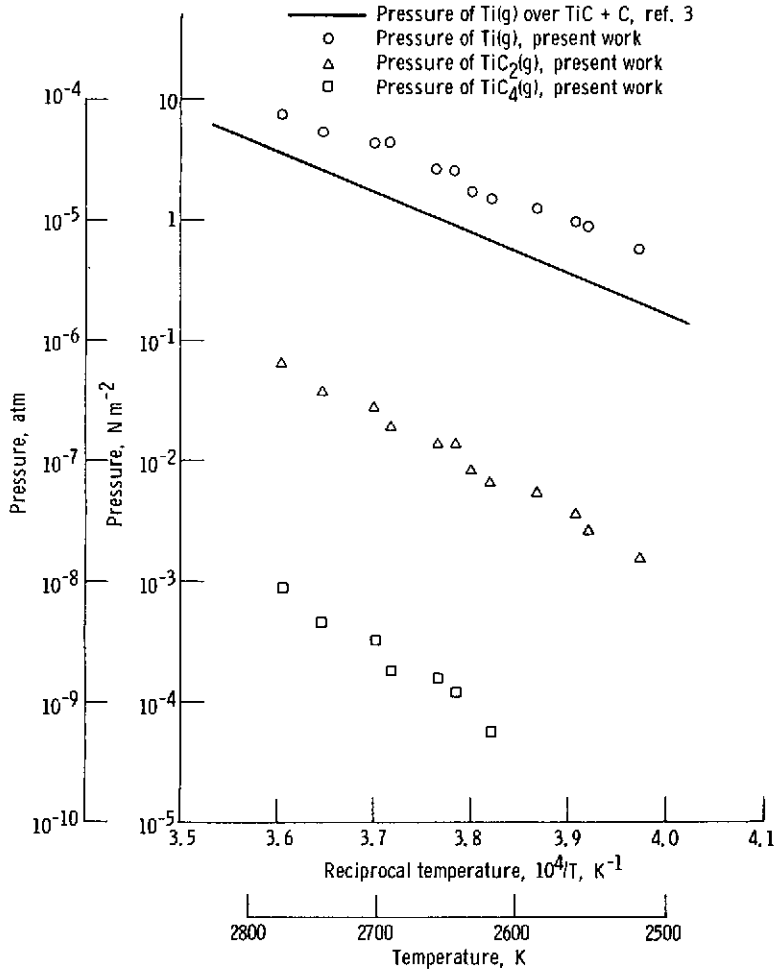

Figure 1. - Partial pressures of Ti, TiC_2, and TiC_4 over TiC + C(s) as a function of reciprocal temperature.

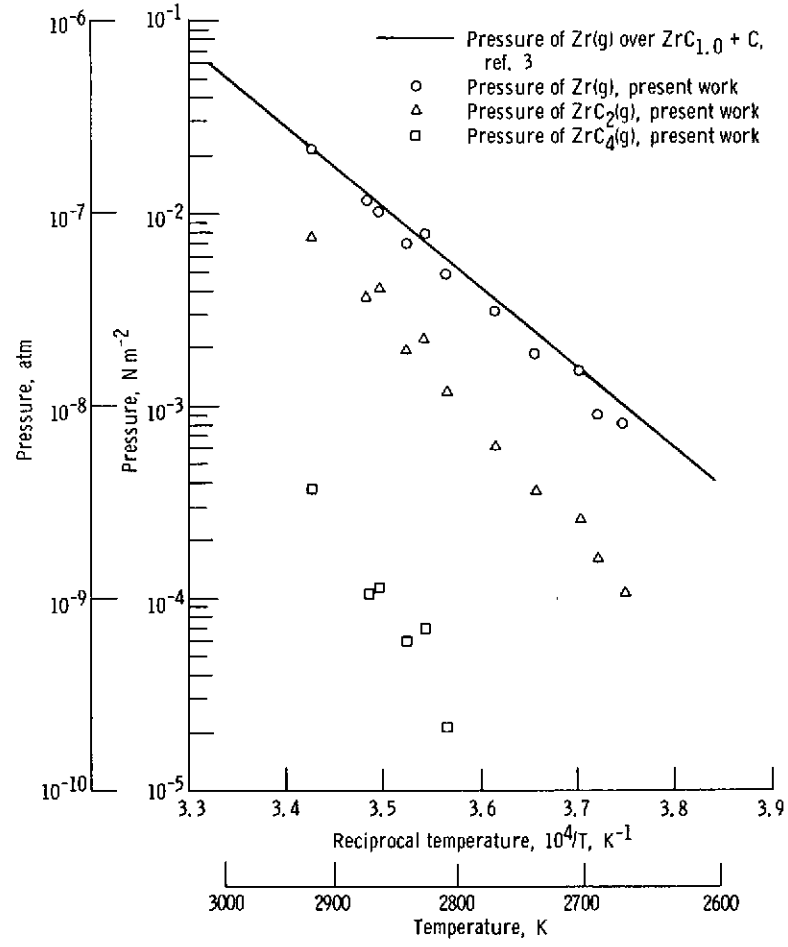

Figure 2. - Partial pressures of Zr, ZrC_2, and ZrC_4 over ZrC + C(s) as function of reciprocal temperature.

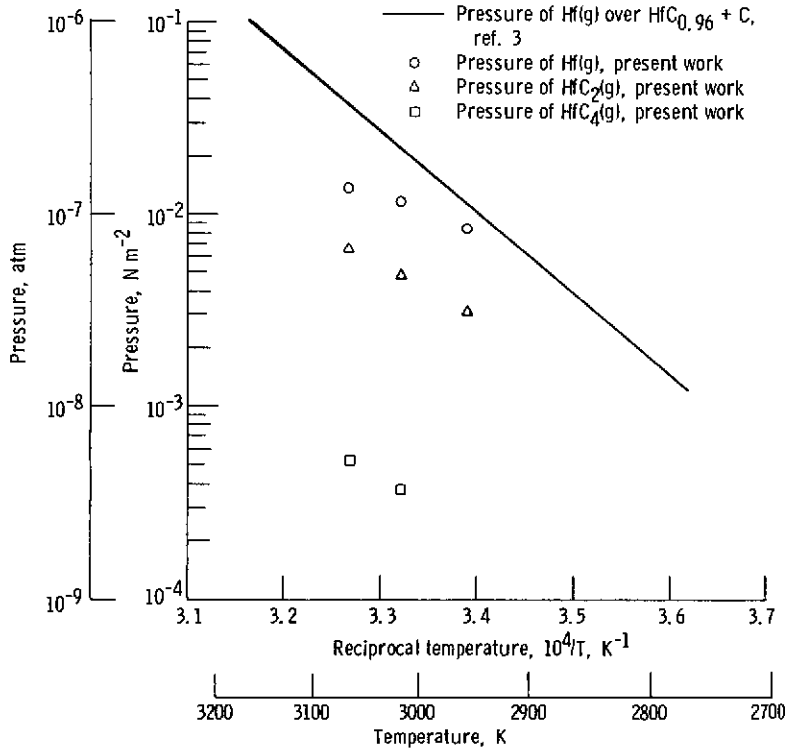

Figure 3. - Partial pressures of Hf, HfC_2, and HfC_4 over HfC + C(s) as a function of reciprocal temperature.

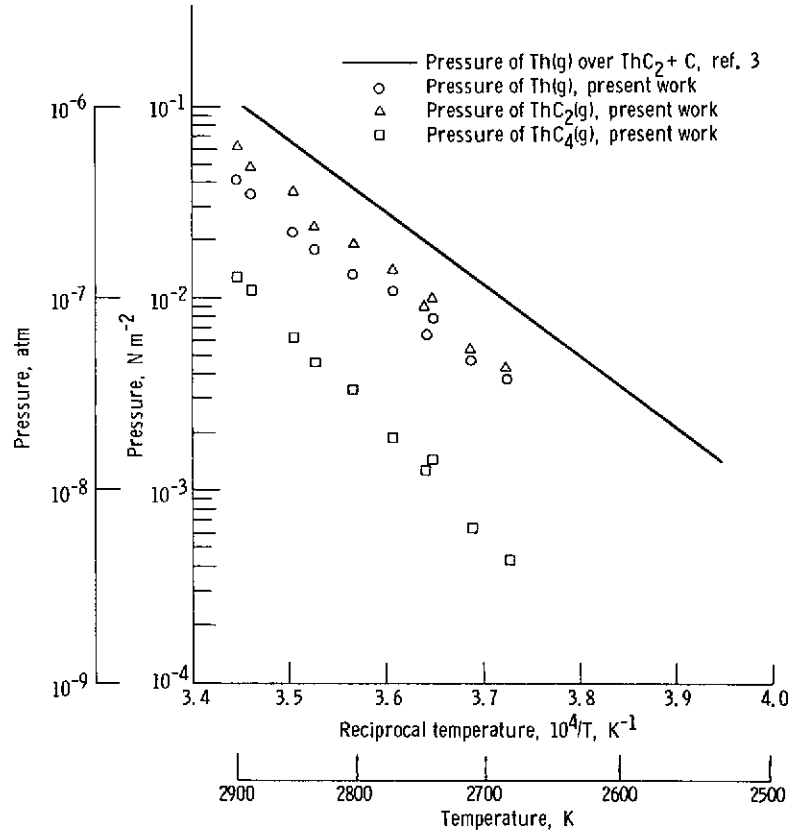

Figure 4. - Partial pressures of Th, ThC_2, and ThC_4 over ThC_2 + C(s) as a function of reciprocal temperature.

The partial pressures (tables 7 to 10 and figs. 1 to 4) of the metal atoms and molecules reported herein are intended to show only the order of magnitude of these pressures. The metal atom pressures are of the same order of magnitude as those compiled by Storms (ref. 3) for the MC + C systems (figs. 1 to 4). We estimated that pressures above 10^{-3} N/m^2 may be in error by a factor of 2, and those below 10^{-3} N/m^2 by a factor of 4. These estimates were based on estimated systematic errors and imprecision in the values of the terms used to calculate P_i from equation (1). The listed pressures pertain strictly to the $MC_x + C$ solid phase, the composition of which is not completely specified in our experiments. Storms has explicitly pointed out that complete knowledge of both the composition (M/C ratio) of the solid phase and the oxide and nitride concentrations is required if absolute values for a thermophysical property such as vapor pressure are to be determined accurately for the metal-carbon systems.

Heats and Entropies of Reactions

Numerous equilibrium reactions may be considered in a thermodynamic analysis of the vaporization of the Group IVB metal-carbon systems. Of primary interest here are the reactions which can lead to a thermodynamic characterization of the molecular dicarbide and tetracarbide species

$$M(g) + xC(s) = MC_x(g) \qquad x = 2 \text{ or } 4 \tag{1}$$

The equilibrium constant K_p for a reaction of this type is given as

$$K_p = P_{MC_x} P_M^{-1} a_C^{-x} \tag{2}$$

where a_C is the activity of the carbon (graphite) in the condensed phase. Reactions of this type are independent of the pressure calibration because K_p is directly proportional to the ratio of the pressures of the gaseous products and reactants. Therefore, for such reactions

$$K_p = \frac{I_{MC_x} E_{MC_x} \sigma_M \gamma_M n_M}{I_M E_M \sigma_{MC_x} \gamma_{MC_x} n_{MC_x}} \tag{3}$$

where the activity of carbon is 1.0 because of the presence of excess graphite powder and the graphite cell liner.

The specific reactions considered here are listed in table 11. The equilibrium constants for reactions 3, 4, 7, and 8 are plotted as a function of reciprocal temperature in figures 5 and 6. For reactions 1 and 2 of table 11 the equilibrium constants are plotted in references 1 and 2.

The lines drawn through the data points are the least-squares fits of the data to an equation of the form

$$\log K_p = \frac{A}{T} + B \tag{4}$$

Second-law enthalpies for reactions 1, 2, 3, 7, and 8 were calculated by use of the van't Hoff equation

$$\Delta H_T^o = -R \, d(\ln K_p) \Big/ d\left(\frac{1}{T}\right) \tag{5}$$

from which the slope of the log K_p against $1/T$ plot is $-\Delta H_T^o/R \ln 10$. The second-law entropy is obtained from the intercept $\Delta S_T^o/R \ln 10$ with the log K_p axis.

TABLE 11. - ENTHALPIES AND ENTROPIES OF REACTIONS

Reaction number	Molecule	Reaction	Temperature range, K	Second-law enthalpy, kJ mol^{-1}		Third-law enthalpy, ΔH_0^o, kJ mol^{-1},	Entropy	
				ΔH_T^o	ΔH_0^o,		Second law, ΔS_T^o J K^{-1} mol^{-1},	Third law, ΔS_T^o J K^{-1} mol^{-1},
1	TiC_2	Ti(g) + 2C(s) = TiC_2(g)	2518 to 2790	242.7±11[a] (T = 2658K)	261.1±23[b]	262.2±20[b]	47.8±4.0[a]	48.2±6.3[b]
2	TiC_4	Ti(g) + 4C(s) = TiC_4(g)	2518 to 2790	443.9±32 (T = 2705)	459.4±68	440.5±22	84.5±12	77.6±6.3
3	ZrC_2	Zr(g) + 2C(s) = ZrC_2(g)	2670 to 3003	235.6±17 (T = 2830)	269.0±27	254.7±24	72.1±5.9	67.1±6.3
4	ZrC_4	Zr(g) + 4C(s) = ZrC_4(g)	2670 to 3003	---	---	369.2±28	---	---
5	HfC_2	Hf(g) + 2C(s) = HfC_2(g)	2952 to 3066	---	---	161.1±27	---	---
6	HfC_4	Hf(g) + 4C(s) = HfC_4 (g)	2952 to 3066	---	---	312.9±23	---	---
7	ThC_2	Th(g) + 2C(s) = ThC_2(g)	2686 to 2906	81.9±18 (T = 2793)	121.3±23	124.3±21	31.7±6.3	32.9±6.3
8	ThC_4	Th(g) + 4C(s) = ThC_4(g)	2686 to 2906	289.0±25 (T = 2793)	322.6±43	255.3±23	90.3±8.9	66.7±6.3

[a]Errors quoted are standard deviations of the slopes and intercepts.

[b]Overall estimated uncertainty. See text. Estimated uncertainties do not include uncertainties from geometry and electronic contribution.

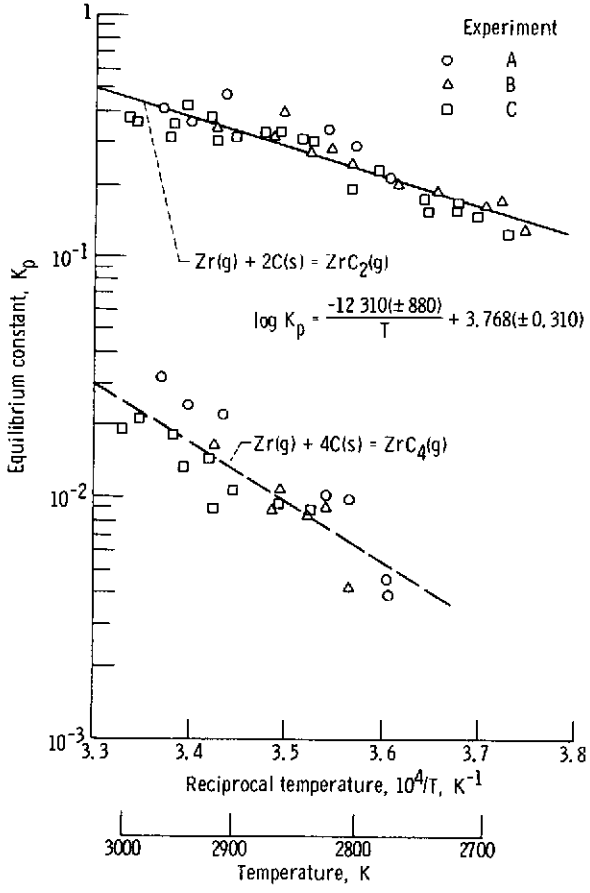

Figure 5. - Equilibrium constants as a function of reciprocal temperature for reactions 3 and 4.

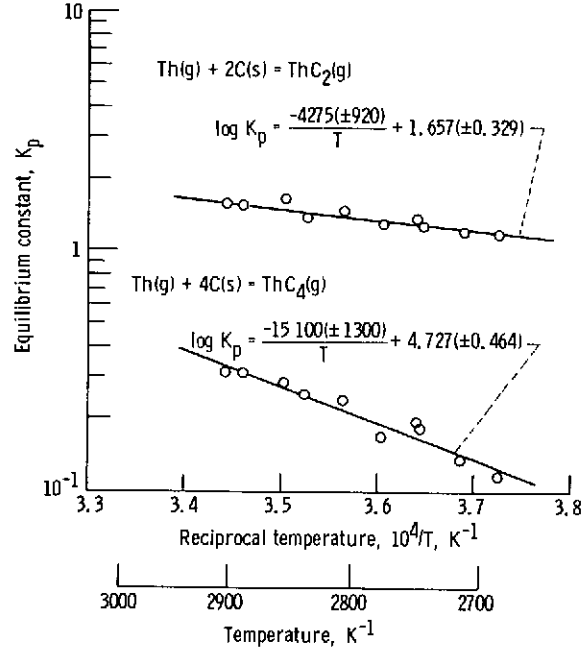

Figure 6. - Equilibrium constants as function of reciprocal temperature for reactions 7 and 8.

For those reactions where no second-law heats and entropies are listed in table 11, either an insufficient number of data points (HfC_2 and HfC_4) or considerable scatter in the data (ZrC_4) precluded the calculation of what we consider to be meaningful values. The ΔH^o_T values were converted to 0 K to obtain second-law heats ΔH^o_0 by use of $H^o_T - H^o_0$ functions for the respective components. The overall uncertainties associated with the ΔH^o_0 values in table 11 were obtained by adding the standard deviation of the slopes to estimated systematic errors of ± 10 kelvin in temperature and ± 4 kJ mol^{-1} in the heat-content functions. The effect of a temperature error on ΔH was obtained by the relation (ref. 32)

$$\delta(\Delta H) = \frac{\sqrt{2}\Delta H\, \delta T}{\Delta T} \tag{6}$$

where $\delta(\Delta H)$ and δT represent the errors in ΔH and T, respectively, and ΔT represents the range of temperature in the experiment.

Third-law enthalpies were calculated at each experimental temperature for all reactions by use of the equation

$$\Delta H^o_0 = -RT \ln K_p - T\,\Delta\left[\frac{G^o_T - H^o_0}{T}\right] \tag{7}$$

where $\Delta\left[(G^o_T - H^o_0)/T\right]$ is the change of the Gibbs free-energy function Δfef for the reaction. Values of the free-energy functions used in our calculations are discussed in the next section. Calculated third-law heats for reactions 1 to 8 are listed in tables 12 to 15, together with other pertinent parameters for each data point. The values of the heats summarized in table 11 are the average of all data points for each reaction. The overall uncertainties listed with these values were obtained by adding the standard deviations of the mean of all respective data points to estimated systematic errors in the values of log K_p (± 0.18), T (± 10 kelvin), and Δfef (± 6.3 J K^{-1} mol^{-1}). The effects of these errors on ΔH are given by (ref. 32)

$$\delta(\Delta H) = \Delta H\left[\left(RT\,\frac{\delta(\ln K_p)}{\Delta H}\right)^2 + \left(T\,\frac{\delta(\Delta fef)}{\Delta H}\right)^2 + \left(\frac{\delta T}{T}\right)^2\right]^{1/2} \tag{8}$$

TABLE 12. - THIRD-LAW ENTHALPIES FOR REACTIONS 1 AND 2

Temperature, K	Logarithm equilibrium constant, $\log_{10} K_p$	Change of Gibbs free-energy function, $-\Delta\left[(G_T^\circ - H_0^\circ)/T\right]$, $J\ K^{-1} mol^{-1}$	Third-law enthalpy, ΔH_0°, $kJ\ mol^{-1}$
Reaction 1: $Ti(g) + 2C(s) = TiC_2(g)$			
2585	-2.348	55.37	259.3
2631	-2.295	55.25	261.0
2644	-2.270	55.22	260.9
2703	-2.191	55.06	262.2
2774	-2.058	54.86	261.5
2741	-2.127	54.96	262.2
2690	-2.220	55.10	262.5
2657	-2.276	55.18	262.4
2618	-2.373	55.28	263.7
2558	-2.433	55.44	261.0
2518	-2.579	55.55	264.2
2551	-2.488	55.46	263.0
2608	-2.355	55.31	261.8
2669	-2.287	55.15	264.1
2725	-2.153	55.00	262.2
2757	-2.134	54.91	264.0
2790	-2.037	54.82	261.7
		Average	262.2±1.3[a]
Reaction 2: $Ti(g) + 4C(s) = TiC_4(g)$			
2644	-4.357	83.35	440.9
2703	-4.124	83.22	438.4
2774	-3.919	83.07	438.6
2741	-4.070	83.14	441.5
2690	-4.254	83.25	443.0
2657	-4.245	83.32	437.3
2618	-4.437	83.40	440.7
2669	-4.332	83.30	443.7
2725	-4.107	83.17	440.9
2757	-4.052	83.10	443.0
2790	-3.857	83.03	437.7
		Average	440.5±2.1[a]

[a]Error is the standard deviation of the points. See text and table 11 for overall estimated uncertainty.

TABLE 13. - THIRD-LAW ENTHALPIES FOR REACTIONS 3 AND 4

Temperature, K	Logarithm equilibrium constant, $\log_{10} K_p$	Change of Gibbs free-energy function, $-\Delta\left[(G_T^o - H_0^o)/T\right]$, $J\ K^{-1}\ mol^{-1}$	Third-law enthalpy, ΔH_0^o, $kJ\ mol^{-1}$
Reaction 3: $Zr(g) + 2C(s) = ZrC_2(g)$			
2773	-0.661	79.13	254.5
2944	- .442	78.41	255.7
2802	- .537	79.01	250.2
2911	- .326	78.55	246.8
2967	- .377	78.32	253.8
2824	- .458	78.92	247.6
2839	- .566	78.85	254.6
2867	- .492	78.73	252.7
2805	- .611	79.00	254.4
2737	- .719	79.28	254.7
2688	- .757	79.49	252.6
2670	- .888	79.57	257.8
2701	- .775	79.44	254.6
2767	- .696	79.16	255.9
2824	- .549	78.92	252.6
2862	- .398	78.75	247.2
2918	- .464	78.52	255.1
2922	- .516	78.50	258.3
2836	- .512	78.87	251.5
2719	- .811	79.36	258.0
2785	- .637	79.08	254.2
2864	- .472	78.74	251.4
2925	- .414	78.49	252.7
2988	- .442	78.24	259.0
2957	- .443	78.36	256.8
3003	- .420	78.18	258.9
2722	- .776	79.35	256.4
2904	- .498	78.57	255.9
2947	- .362	78.40	251.5
2875	- .477	78.70	252.5
2842	- .506	78.84	251.6
2681	- .898	79.52	259.3
2705	- .821	79.42	257.4
2743	- .788	79.26	258.8
2747	- .762	79.24	257.7
2806	- .716	78.99	260.1
2960	- .496	78.35	260.0
		Average	254.7±3.5[a]

Temperature, K	Logarithm equilibrium constant, $\log_{10} K_p$	Change of Gibbs free-energy function, $-\Delta\left[(G_T^o - H_0^o)/T\right]$, $J\ K^{-1}\ mol^{-1}$	Third-law enthalpy, ΔH_0^o, $kJ\ mol^{-1}$
Reaction 4: $Zr(g) + 4C(s) = ZrC_4(g)$			
2775	-2.346	91.19	377.7
2773	-2.399	91.19	380.2
2944	-1.609	90.76	357.9
2802	-2.003	91.12	362.8
2911	-1.656	90.84	356.7
2967	-1.498	90.71	354.2
2824	-1.995	91.07	365.0
2839	-2.070	91.03	370.9
2867	-2.048	90.96	373.2
2805	-2.370	91.12	382.8
2824	-2.043	91.07	367.6
2862	-1.959	90.97	367.7
2918	-1.771	90.83	364.0
2922	-2.048	90.82	379.9
2836	-2.049	91.04	369.4
2864	-2.030	90.96	371.8
2925	-1.846	90.81	369.0
2988	-1.677	90.66	366.8
2957	-1.738	90.73	366.7
3003	-1.711	90.62	370.5
2904	-1.972	90.86	373.5
2947	-1.880	90.76	373.5
		Average	369.2±7.3[a]

[a]Error is the standard deviation of the points. See text and table 11 for overall estimated uncertainty.

TABLE 14. - THIRD-LAW ENTHALPIES FOR REACTIONS 5 AND 6

Temperature, K	Logarithm equilibrium constant, $\log_{10} K_p$	Change of Gibbs free-energy function, $-\Delta\left[(G_T^o - H_0^o)/T\right]$, $J\ K^{-1} mol^{-1}$	Third-law enthalpy, ΔH_0^o, $kJ\ mol^{-1}$
Reaction 5: $Hf(g) + 2C(s) = HfC_2(g)$			
2952	-0.428	45.53	158.6
3013	-.372	45.28	157.9
3066	-.323	45.10	157.3
3030	-.580	45.23	170.7
		Average	161.1±5.6[a]
Reaction 6: $Hf(g) + 4C(s) = HfC_4(g)$			
3013	-1.486	75.13	312.1
3066	-1.427	74.98	313.6
		Average	312.9±0.8[a]

[a]Error is the standard deviation of the points. See text and table 11 for overall estimated uncertainty.

TABLE 15. - THIRD-LAW ENTHALPIES FOR REACTIONS 7 AND 8

Temperature, K	Logarithm equilibrium constant, $\log_{10} K_p$	Change of Gibbs free-energy function, $-\Delta[(G_T^o - H_0^o)/T]$, $J\,K^{-1}mol^{-1}$	Third law enthalpy, ΔH^o_0, $kJ\,mol^{-1}$
Reaction 7: $Th(g) + 2C(s) = ThC_2(g)$			
2742	0.094	47.19	124.5
2686	.057	47.48	124.6
2711	.062	47.35	125.2
2747	.131	47.17	122.7
2773	.099	47.03	125.2
2837	.131	46.69	125.4
2855	.215	46.60	121.3
2890	.143	46.41	126.2
2906	.175	46.33	124.9
2804	.160	46.87	122.9
		Average	124.3±1.4[a]
Reaction 8: $Th(g) + 4C(s) = ThC_4(g)$			
2742	-0.741	78.66	254.6
2686	- .933	78.90	259.9
2711	- .872	78.79	258.9
2747	- .712	78.63	253.4
2773	- .768	78.52	258.5
2837	- .592	78.23	254.1
2855	- .543	78.15	252.8
2890	- .507	78.00	253.5
2906	- .506	77.93	254.6
2804	- .607	78.38	252.4
		Average	255.3±2.6[a]

[a]Error is the standard deviation of the points. See text and table 11 for overall estimated uncertainty.

Molecular Constants and Thermodynamic Functions

Numerical values of the thermodynamic functions (enthalpy, entropy, and free-energy functions) for the chemical species considered herein are needed for second- and third-law treatments of ion intensity or pressure data. Whenever possible these values were taken from either the JANAF tables (ref. 33, Ti(g), Zr(g), C(s)) or Hultgren's compilation (ref. 30, Hf(g) and Th(g)).

The thermodynamic functions for the molecules were calculated on the basis of assumed molecular structures and estimated molecular parameters. Because the derived values of the functions have a significant influence on the values of the third-law heats, it is essential that the bases for deriving these functions be enumerated. Tables 16 and 17 list the estimated parameters used. In the absence of experimentally established structures, we initially assumed a linear asymmetric structure of the type M-C-C for the dicarbides by analogy to other metal dicarbides. For reasons presented later in this section, this structure was deemed acceptable for TiC_2, HfC_2, and ThC_2 but not necessarily appropriate for ZrC_2. Therefore, for ZrC_2, asymmetric bent and symmetric linear and bent structures were also considered. A bent asymmetric structure with an apex angle of 120° was finally used for $ZrC_2(g)$. The bent structure added 17.2 J K^{-1} mol^{-1} more to the free-energy functions at 3000 K than did the linear asymmetric structure. The bent structure for ZrC_2 is contrary to the results of the application of Walsh's rule for the triatomic molecules (ref. 34) which predicts that a molecule with 6 valence electrons should be linear. For all the tetracarbide molecular species a linear symmetric structure of the type C-C-M-C-C was assumed.

TABLE 16. - BASES FOR THERMODYNAMIC FUNCTIONS

	Molecule				
	TiC_2	ZrC_2	HfC_2	ThC_2	MC_4
Symmetry	$C_{\infty v}$	$C_{\infty v}$ $^{a}C_{s,\,120^{\circ}}$	$C_{\infty v}$	$C_{\infty v}$	$D_{\infty h}$
Interatomic distance[b], r_{M-C}, nm (Å)	0.163 (1.63)	0.175 (1.75)	0.177 (1.77)	0.190 (1.90)	M-C same as MC_2
Possible electronic contributions	$^{1}\Sigma^{+}$ TiO states ($^{3}\Delta$ ground state)[a] Ti^{+2} states	$^{1}\Sigma^{+}$ ZrO states ($^{1}\Sigma^{+}$ ground state) Zr^{+2} states[a]	$^{1}\Sigma^{+}$[a] Hf^{+2} states	$^{1}\Sigma^{+}$[a] Th^{+2} states	Same as MC_2

[a]Final selection.

[b]M-C interatomic distance estimated by comparison with corresponding M-O distance and force constant (refs. 35 and 36). C-C interatomic distance equal to 0.131 nm (1.31 Å), taken from $C_2(g)$ (ref. 61).

TABLE 17. - MOMENTS OF INERTIA, FORCE CONSTANTS, AND VIBRATIONAL FREQUENCIES

	Molecule								
	TiC_2	TiC_4	ZrC_2 ($C_{\infty v}$)	ZrC_2 ($C_{s,\ 120^o}$)	ZrC_4	HfC_2	HfC_4	ThC_2	ThC_4
Moment of inertia, (g)(cm^2)	15.58×10^{-39}	45.07×10^{-39}	19.97×10^{-39}	203.0×10^{-117} ($I_a I_b I_c$)	49.56×10^{-39}	22.38×10^{-39}	50.34×10^{-39}	25.30×10^{-39}	55.50×10^{-39}
Force constants, N m^{-1}									
k^a_{M-C}	7.18×10^2	7.18×10^2	7.03×10^2	7.03×10^2	7.03×10^2	6.93×10^2	6.93×10^2	5.50×10^2	5.50×10^2
k^b_{C-C}	9.25	9.25	9.25	9.25	9.25	9.25	9.25	9.25	9.25
k_δ, Nm/rad[c]	6.70×10^{-19}	----------	6.70×10^{-19}	6.70×10^{-19}	----------	6.70×10^{-19}	----------	6.70×10^{-19}	----------
$f^d_{13,22}$	----------	1.30×10^2	----------	----------	1.30	----------	1.30	----------	1.30
Frequencies (degeneracy)[e], cm^{-1}:									
ω_1	780	808	713	1003	804	673	801	605	761
ω_2	494(2)	1878	477(2)	329	1874	474(2)	1872	463(2)	1836
ω_3	1810	1020	1797	1677	891	1791	812	1751	734
ω_4	------	1836	------	----	1818	------	1810	------	1771
ω_5(2)	------	137	------	----	118	------	108	------	101
ω_6(2)	------	573	------	----	531	------	516	------	494
ω_7(2)	------	468	------	----	454	------	453	------	437
Symmetry number	1	2	1	1	2	1	2	1	2

[a]Stretching force constants for Ti-, Zr-, and Hf-C were assumed to be the same as those of the corresponding oxides (ref. 61); for Th-C, value taken from ref. 22 was used.

[b]From C_2(g) (ref. 61).

[c]Ref. 37 for bending force constant.

[d]Ref. 38.

[e]The fundamental vibrational frequencies were calculated according to the valence force formulation (refs. 37 and 38).

The interatomic distances M-C were estimated on the basis of values reported for the corresponding metal monoxides (refs. 35 and 36). Vibrational frequencies were calculated by use of the valence force approximation formulation (refs. 37 and 38) with estimated force constants derived from oxides and the C_2 molecule. The bending force constant was estimated by considering those determined for other triatomic molecules.

In addition to the paucity of experimental data on molecular geometry, the electronic contribution to the partition function is unknown for the molecules being studied. Therefore, we considered three separate methods of estimating the electronic contributions. The first and simplest alternative is to assume a $^1\Sigma^+$ ground state, which results in a zero electronic contribution. This assumption is based on the postulate that the bonding of the C_2^{-2} group is simular to O^{-2} and the fact that $^1\Sigma^+$ is the ground state for ZrO, HfO, and ThO (ref. 35).

The second possibility is to consider electronic contributions from the ground state and low-lying excited states. The observed and estimated electronic energy levels for TiO and ZrO have been discussed by Brewer and Green (ref. 39). The ground state for TiO is a $^3\Delta$; and the low-lying excited states are $^1\Delta$ (600 cm^{-1}), $^1\Sigma^+$(2800 cm^{-1}), $^3\Pi$ (9000 cm^{-1}), and $^1\Pi$ (11 900 cm^{-1}). For ZrO the ground state is $^1\Sigma^+$; and $^3\Delta$ (1000 cm^{-1}), $^1\Delta$ (5000 cm^{-1}), $^3\Pi$ (8000 cm^{-1}), and $^1\Pi$(11 000 cm^{-1}) are the excited states. When these electronic levels for TiC_2 and ZrC_2 are used, the electronic contribution to the free-energy functions at 3000 K are 17.2 and 13.4 J $K^{-1}mol^{-1}$, respectively. Excited states for HfO and ThO are not known, so similar consideration could not easily be applied to HfC_2 or ThC_2.

The third alternative is to assume that the energy levels of the molecule can be approximated by those of the M^{+2} ions. This method, as used by Brewer and Rosenblatt for metal oxides (ref. 40), is based on an ionic model of the type $M^{+2}C_2^{-2}$ and assumes that the C_2^{-2} ion neither makes an electronic contribution to the partition function nor perturbs the energy levels of M^{+2}. The energy levels used for M^{+2} were taken from reference 40. At 3000 K the contributions to the free-energy functions are 24.3, 22.6, 20.1, and 25.9 J $K^{-1}mol^{-1}$ for TiC_2, ZrC_2, HfC_2, and ThC_2, respectively.

Our final selections of structures and electronic contributions used in deriving the thermodynamic functions were made by comparing second- and third-law enthalpies and entropies of reaction. For TiC_2 the thermodynamic functions were derived for a linear asymmetric structure with an electronic contribution of the TiO states. (Only the $^3\Delta$ ground state is considered in refs. 1 and 2). This particular combination was found to yield the best second- and third-law agreement (table 11).

For the reaction involving ZrC_2, it was decided to use the asymmetric structure bent 120° plus the electronic contribution for the Zr^{+2} states. This combination resulted in the best agreement between the calculated enthalpies and entropies.

TABLE 18. - THERMODYNAMIC FUNCTIONS FOR MC_2 AND MC_4 MOLECULES

Temperature, K	Heat content, $H_T^\circ - H_0^\circ$, kJ mol^{-1}	Entropy S_T°, J K^{-1} mol^{-1}	Free-energy function, $-(G_T^\circ - H_0^\circ)/T$, J K^{-1} mol^{-1}	Heat content, $H_T^\circ - H_0^\circ$, kJ mol^{-1}	Entropy S_T°, J K^{-1} mol^{-1}	Free-energy function, $-(G_T^\circ - H_0^\circ)/T$, J K^{-1} mol^{-1}
	$TiC_2(g)$			$TiC_4(g)$		
298.15	10.23	251.07	216.75	14.83	286.57	236.84
2400	133.38	367.30	311.72	230.42	487.42	391.41
2500	139.68	369.87	314.00	241.58	491.98	395.34
2600	146.00	372.35	316.19	252.78	496.37	399.14
2700	152.34	374.74	318.32	264.00	500.60	402.82
2800	158.69	377.05	320.37	275.24	504.69	406.39
2900	165.06	379.28	322.37	286.51	508.64	409.85
3000	171.45	381.45	324.30	297.80	512.47	413.21
3100	177.85	383.55	326.18	309.11	516.18	416.47
3200	184.26	385.58	328.00	320.44	519.78	419.64
	$ZrC_2(g)$			$ZrC_4(g)$		
298.15	11.46	281.90	243.48	15.57	295.50	243.39
2400	132.96	398.83	343.43	238.38	505.80	406.47
2500	138.99	401.30	345.70	249.69	510.42	410.54
2600	145.04	403.67	347.88	261.03	514.86	414.47
2700	151.10	405.95	349.99	272.39	519.15	418.26
2800	157.17	408.16	352.03	283.77	523.29	421.94
2900	163.26	410.30	354.00	295.17	527.29	425.50
3000	169.36	412.37	355.92	306.60	531.16	428.96
3100	175.48	414.37	357.76	318.04	534.91	432.32
3200	181.61	416.32	359.57	329.50	538.55	435.58
	$HfC_2(g)$			$HfC_4(g)$		
298.15	10.29	252.44	217.93	15.35	288.43	236.95
2400	131.67	367.25	312.39	230.15	489.38	393.49
2500	137.81	369.76	314.63	241.17	493.88	397.41
2600	143.96	372.17	316.80	252.20	498.21	401.21
2700	150.11	374.49	318.89	263.25	502.38	404.88
2800	156.27	376.73	320.92	274.31	506.40	408.43
2900	162.44	378.89	322.88	285.38	510.28	411.88
3000	168.61	380.99	324.78	296.46	514.04	415.22
3100	174.78	383.01	326.63	307.55	517.68	418.47
3200	180.96	384.97	328.42	318.64	521.20	421.62
	$ThC_2(g)$			$ThC_4(g)$		
298.15	10.42	257.07	222.11	15.67	294.29	241.71
2400	132.30	372.63	317.50	231.54	496.83	400.35
2500	138.45	375.14	319.76	242.57	501.33	404.30
2600	144.60	377.55	321.94	253.62	505.66	408.12
2700	150.76	379.88	324.04	264.67	509.84	411.81
2800	156.93	382.12	326.07	275.74	513.86	415.38
2900	163.10	384.28	328.04	286.82	517.75	418.85
3000	169.27	386.38	329.95	297.91	521.51	422.21
3100	175.45	388.40	331.81	309.00	525.15	425.47
3200	181.63	390.36	333.61	320.11	528.67	428.64

Thermodynamic functions for ThC_2 were derived by using the linear asymmetric structure and the $^1\Sigma^+$ ground state. Because the number of data points for the HfC_2 reaction was insufficient for a second-law treatment and a third-law comparison, the HfC_2 functions were obtained on bases similar to those used for ThC_2, namely, linear asymmetric structure and $^1\Sigma^+$ ground state.

For the tetracarbide molecules, even less definitive structural information is available than for the dicarbides. Therefore, as mentioned previously, we assumed linear symmetric structures for these molecules in all cases. Electronic contributions identical to the respective metal dicarbides were used for each tetracarbide.

Thermodynamic functions were calculated with a NASA computer program (ref. 41) and the rigid-rotator harmonic oscillator approximation. Heat contents, entropies, and free-energy functions for the metal dicarbide and tetracarbide molecules are listed in table 18.

Dissociation Energies and Heats of Formation

The dissociation energies, atomization energies, and heats of formation for the dicarbides and tetracarbides listed in table 19 were calculated by combining the third-law heats of reaction with the heats of formation of C(g)(709.5±1.9 kJ mol^{-1}, ref. 33)

TABLE 19. - DISSOCIATION ENERGIES AND HEATS OF FORMATION OF MC_2 AND MC_4 MOLECULES

Molecule	Dissociation energy, D_0^o (M-C_2), kJ mol^{-1}	Atomization energy, D_0^o (M-C-C), kJ mol^{-1}	Heat of formation, ΔH_0^o, kJ mol^{-1}
TiC_2	567.1±21	1157±21	732.5±21
ZrC_2	574.6±24	1164±24	873.9±28
HfC_2	668.2±28	1258±28	779.9±28
ThC_2	705.0±22	1295±22	700.0±22
	D_0^o (C_2-M-C_2)	D_0^o(C-C-M-C-C)	
TiC_4	1218±22	2398±22	910.8±22
ZrC_4	1289±28	2469±28	988.4±31
HfC_4	1346±23	2525±23	931.7±23
ThC_4	1403±23	2583±23	831.0±23

and $C_2(g)$(829.3±3.8 kJ mol^{-1}, ref. 33) and the heats of formation of the gaseous metals Ti(470.3±4.2 kJ mol^{-1}, ref. 33), Zr(619.2±14.6 kJ mol^{-1}, ref. 33), Hf(618.8±4.2 kJ mol^{-1}, ref. 30), and Th(575.7±2.1 kJ mol^{-1}, ref. 30). Even for cases where second-law heats were available, the third-law values were used because they had generally smaller estimated errors exclusive of the uncertainty in electronic contributions to the thermodynamic functions.

Although the metal dicarbide and tetracarbide molecules are the species of major interest, a small amount of data was also obtained which can be used to determine maximum values for the dissociation energies of the metal monocarbide molecules.

An approximate value for the dissociation energy of ThC(g) was obtained, and maximum values were calculated for the TiC(g), ZrC(g), and HfC(g) molecules by use of the reaction

$$M(g) + C(s) = MC(g)$$

With the assumption that the parent molecular ion of TiC^+ existed just below our level of detectability, a maximum value of 432±25 kJ mol^{-1} was calculated for the TiC (ω_e = 1126 cm^{-1}, $^1\Sigma$ ground state) dissociation energy D_0°. If we assume that all the observed ZrC^+ and HfC^+ ions (tables 3 and 4) are parents and calculate maximum values of D_0° for ZrC (ω_e = 1060 cm^{-1}, $^1\Sigma$ ground state) and HfC (ω_e = 1022 cm^{-1}, $^1\Sigma$ ground state), we obtain 556±25 and 536±25 kJ mol^{-1}, respectively. From two data sets obtained with the ThC^+ ion, a dissociation energy of 483±25 kJ mol^{-1} was calculated for ThC (ω_e = 904 cm^{-1}, $^1\Sigma$ ground state). Gingerich (ref. 15) has estimated that the dissociation energies for the TiC, ZrC, HfC, and ThC molecules are 473, 527, 544, and 485 kJ mol^{-1}, respectively (all with an estimated uncertainty of ±63 kJ mol^{-1}). Each of these estimates are in approximate agreement with the present experimental determinations. Insufficient data were available to determine an atomization energy for $ThC_3(g)$ or the possible parent molecules $ZrC_3(g)$ or $HfC_3(g)$.

DISCUSSION

The results of the experiments on the vaporization of the Group IVB metal-carbon systems demonstrate that, in addition to the metal atoms and carbon polymers, the metal-carbon molecules are important species in the vapor phase. In table 20 the concentration ratios of M/MC_x are listed for the systems studied together with the ratios for systems in neighboring groups. Within Group IVB, it is apparent that the abundance of the carbide species increases as the molecular weight increases. This

TABLE 20. - ABUNDANCE RATIOS OF CARBIDE VAPORIZATION SPECIES

Group IIIB	Group IVB	Group VB	Group VIB
$Sc/ScC_2 = 6\times10^2$ $Sc/ScC_4 = 2\times10^5$ (2300 K)	$Ti/TiC_2 = 4\times10^2$ $Ti/TiC_4 = 6\times10^4$ (2500 K)	$V/VC_2 = 8\times10^2$ $V/VC_4 = 3\times10^5$ (2500 K)	$Cr/CrC_2 = 1\times10^6$ (2100 K)
$Y/YC_2 = 8$ $Y/YC_4 = 8\times10^2$ (2500 K)	$Zr/ZrCr = 4$ $Zr/ZrC_4 = 1\times10^2$ (2800 K)	[a] $Nb/NbC_2 = 40$ (2500 K)	Mo
$La/LaC_2 = 2$ $La/LaC_3 = 8\times10^2$ $La/LaC_4 = 70$ (2500 K)	$Hf/HfC_2 = 3$ $Hf/HfC_4 = 30$ (3000 K)	[b] $Ta/TaC_2 \cong 2\times10^2$ (3000 K)	W
	$Th/ThC_2 = 7\times10^{-1}$ $Th/ThC_3 \geq 50$ $Th/ThC_4 = 5$ (2700 K)		[c] $U/UC_2 = 4$ $U/UC_4 = 3\times10^2$ (2450 K)

[a] Ref. 6.

[b] Not an equilibrium value.

[c] Ref. 62.

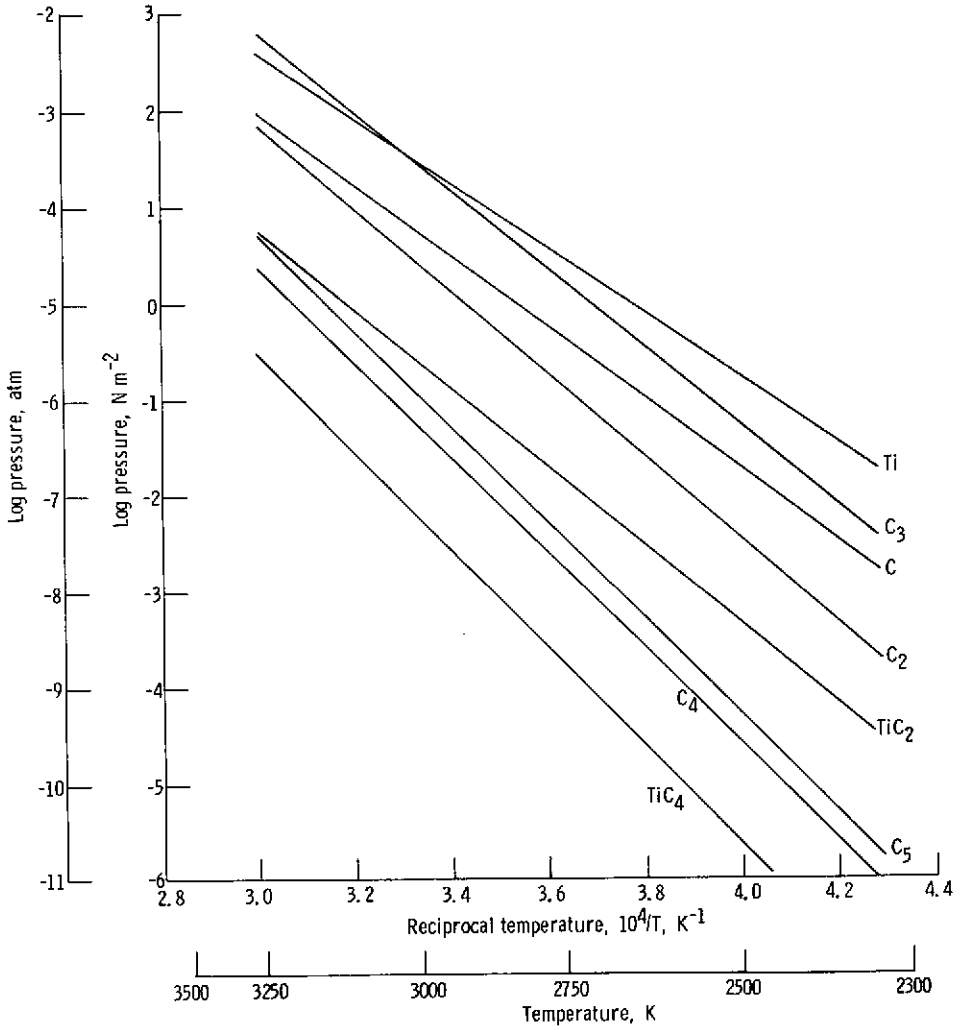

Figure 7. - Partial pressure of species over TiC + C(s) system.

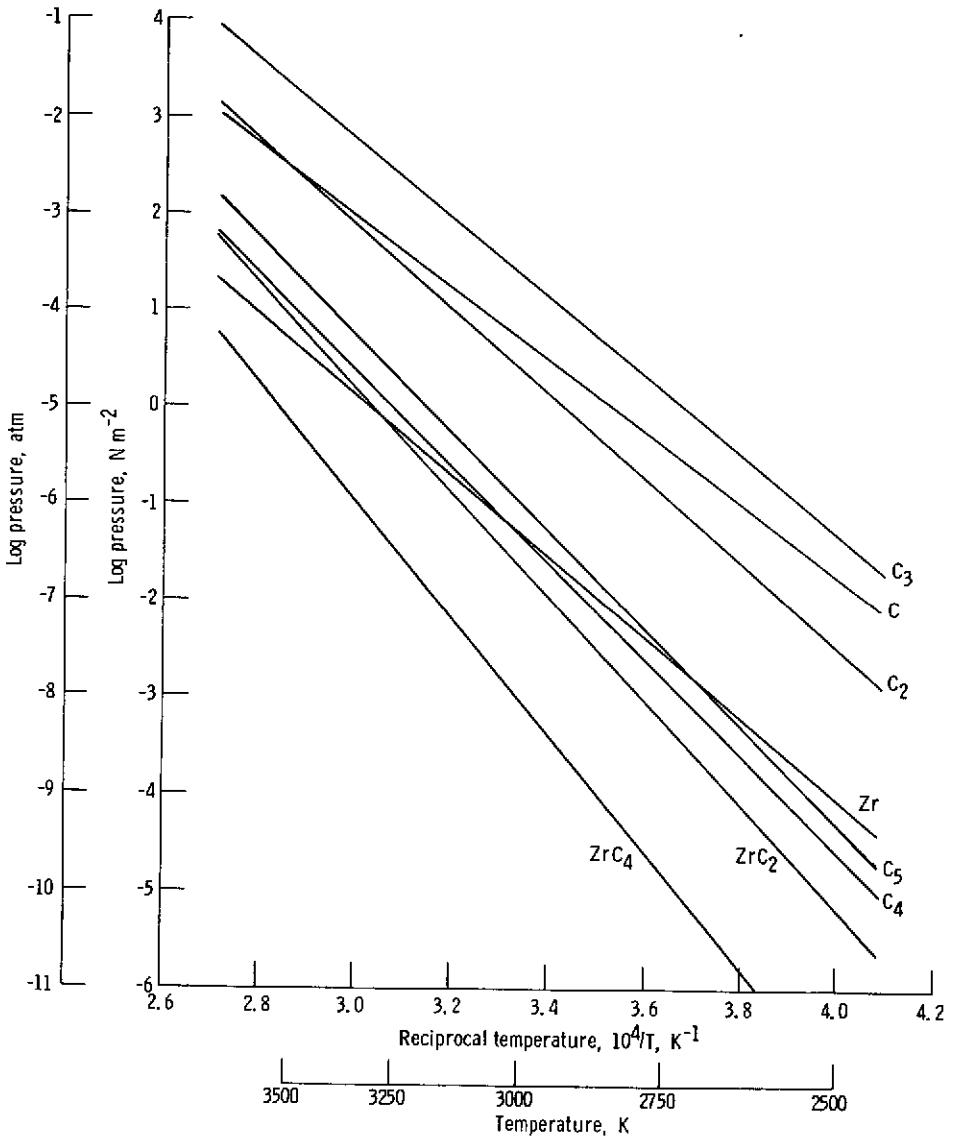

Figure 8. - Partial pressures of species over ZrC + C(s) system.

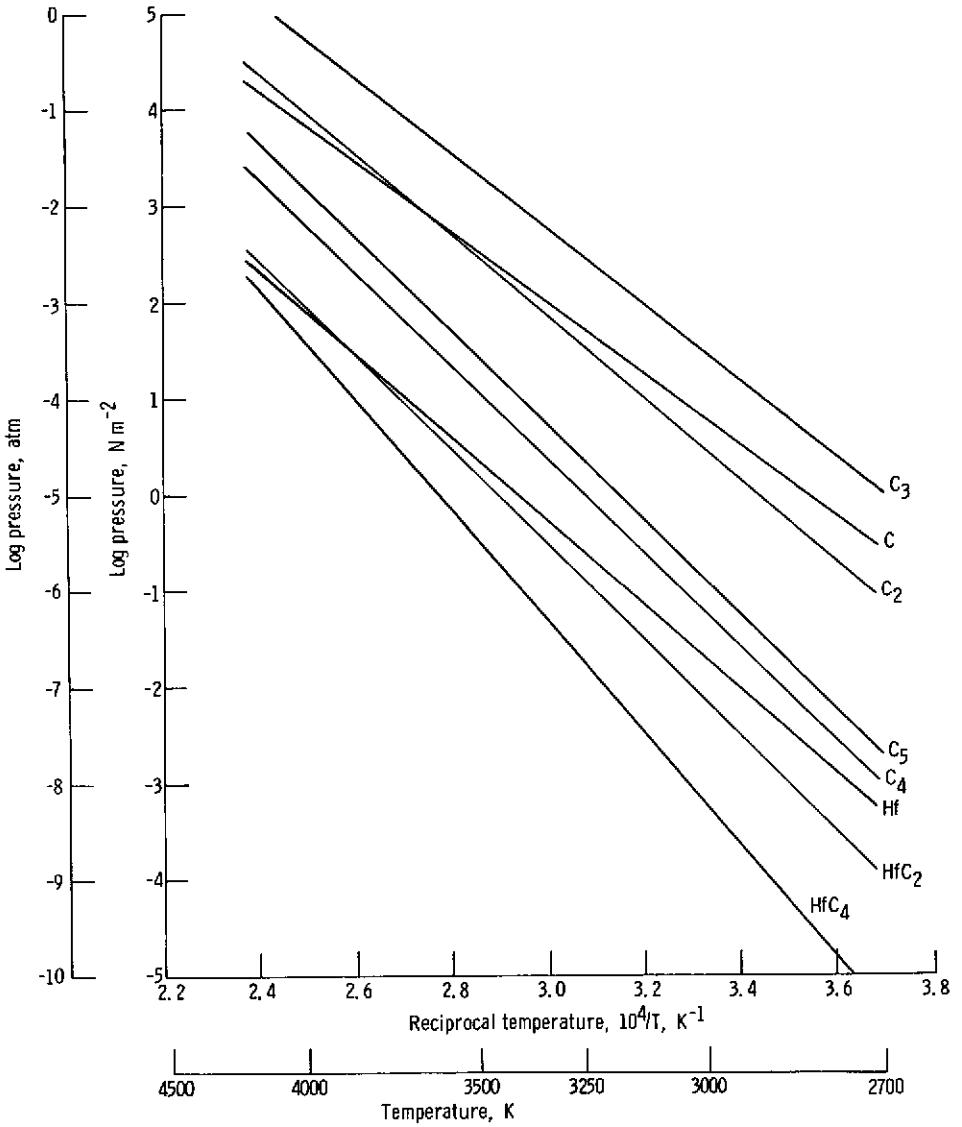

Figure 9. - Partial pressures of species over HfC + C(s) system.

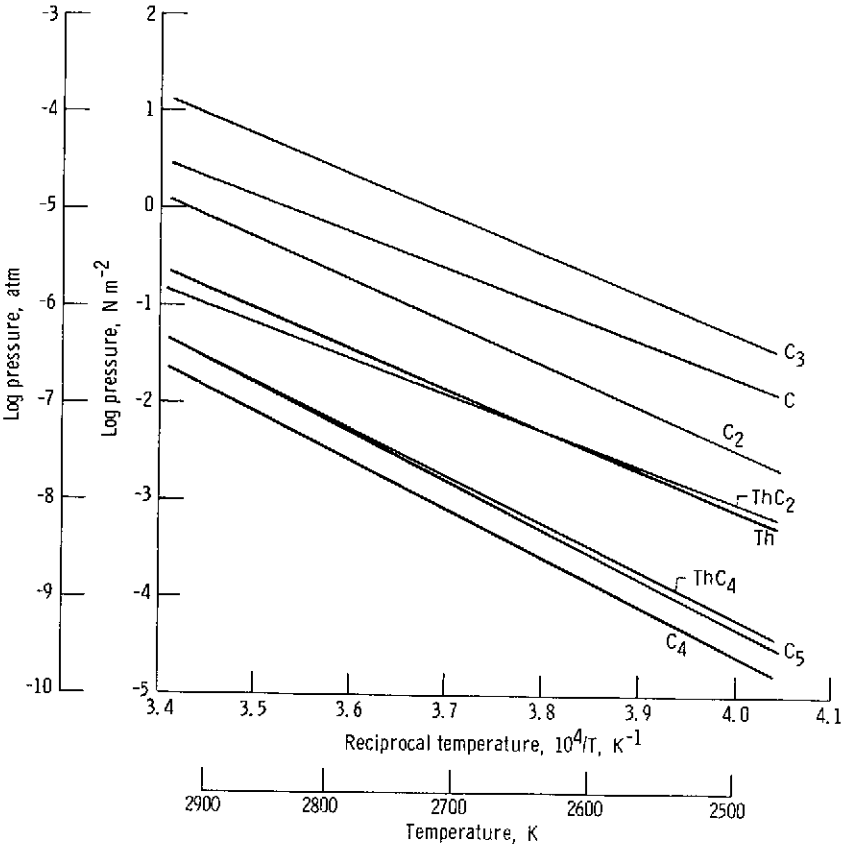

Figure 10. - Partial pressure of species over ThC_2 + C(s) system.

same trend can be recognized in the neighboring groups of elements. The table clearly shows that for the heavier elements the molecular species become significant vaporization products. The trends in the equilibrium constants as a function of temperature for the reactions considered in the preceding paragraphs indicate that as the temperature is increased the carbide species become more important. In figures 7 to 10 we have plotted the partial pressures of M, MC_2, MC_4 and the carbon polymers (ref. 33) for the MC_x + C phases to the MC_x phase melting points. The increases in relative importance of the metal-carbon molecules with temperature, although not dramatic, is apparent from these plots.

The thermodynamic data for the molecular carbide species may aid in the determination of some thermodynamic properties of the condensed-phase metal carbides. The resultant knowledge of the activities of C and M as a function of composition of a particular phase and the derived thermodynamic parameters such as the heats, entropies, and free energies of formation can then be used to test the various models proposed for the chemical bonding of these phases. For an equilibrium reaction of the type

$$M(g) + 2C(MC_x(s)) = MC_2(g)$$

It is apparent that the ratio of pressures of MC_2 to M or the ratio of mass spectrometrically determined ion intensities $I_{MC_2^+}/I_{M^+}$ is proportional to the activity squared of carbon:

$$a_C^2 = \frac{1}{K_p} \frac{P_{MC_2}}{P_M} \cong \frac{1}{K_p} \frac{I_{MC_2^+}}{I_{M^+}} \tag{9}$$

Once the equilibrium constant K_p has been established for the reaction with carbon at unit activity (as in the present study), subsequent measurements of $I_{MC_2^+}/I_{M^+}$ for samples with reduced carbon content can be used to determine this activity as a function of composition. It has been pointed out previously (ref. 42 and refs. cited therein) that such a technique should eliminate some of the difficulties and uncertainties introduced when absolute vapor pressure measurements are made first on a pure element and then on a compound with the element at reduced activity.

A comparison of the bond dissociation energies for the carbides with those for the corresponding oxides (ref. 32) as shown in table 21 provides some interesting insights. In each case the strength of the M-O bond is greater than that of the corresponding $M-C_2$ bond. Likewise, the dioxide dissociation energy is greater than that of the corresponding metal tetracarbide. Similar comparisons for other metal-carbon and metal-oxygen systems have shown that the metal-carbon bonds are some 40 to 120 kJ weaker than the corresponding metal-oxygen bond. From table 21, it is apparent that this tendency holds for all the molecules of Group IVB metals except Zr. The difference in bond strengths for the Zr carbides is greater than 180 kJ.

TABLE 21. - BOND ENERGIES FOR GROUP IVB METAL OXIDES[a] AND DICARBIDES

Bond energy, KJ mol^{-1}	Ti	Zr	Hf	Th
D_0^o (M-O)	661±21	757±21	766±25	828±21
D_0^o ($M-C_2$)	567±21	575±24	668±28	705±22
D_0^o (O-M-O)	1310±21	1443±42	1506±83	1623±21
D_0^o (C_2-M-C_2)	1218±22	1289±28	1346±23	1403±23

[a]Ref. 32.

CONCLUDING REMARKS

Thermodynamic circumstances dictate that the metal carbide molecules of the Group IVB elements are important components of the high-temperature vapors of these materials. There is some uncertainty in the derived thermodynamic parameters because of a lack of information concerning the molecular constants and structures. It would be fruitful to obtain more accurate thermodynamic information by means of a second-law treatment of data from exchange reactions between various carbide molecules. One of the well-established species such as LaC_2, CeC_2, or TiC_2 could be used as a reference molecule in a second-law treatment. This procedure would eliminate uncertainty in the derived thermodynamic quantity caused by uncertainties in free-energy functions used in third-law calculations. In addition, the lack of experimentally determined geometric and electronic structural parameters for these molecules makes this family an ideal one on which to perform sophisticated theoretical and experimental investigations. Further investigation would be particularly worthwhile for the case of $ZrC_2(g)$ to test the structure proposed herein.

Lewis Research Center,
National Aeronautics and Space Administration,
Cleveland, Ohio, October 19, 1973,
502-01.

APPENDIX - KNUDSEN CELL INLET SYSTEM AND MASS SPECTROMETER

The apparatus consists of a Knudsen cell molecular beam inlet system coupled to a modified commercial (Consolidated Electrodynamics Corp. Model 21-110) Mattauch-Herzog type double-focusing mass spectrometer. This facility provides the unique capability for investigating, at high mass resolution and high sensitivity, the vaporization thermodynamics of materials at temperatures to 3300 K. The sensitivity and dynamic range of the apparatus permit the measurement of equilibrium partial pressures in a Knudsen cell over the range from 10^{2} to 10^{-6} N/m^{2} (10^{-3} to 10^{-11} atm) with a mass resolution for the analyzer of at least 2000. This resolution, based on the 10 percent valley definition (ref. 43), is considered high for vaporization thermodynamic studies. But it was found to be essential for identifying and measuring some molecular species (refs. 26 to 29). An overall schematic representation of our apparatus is shown in figure 11. A complete set of engineering drawings of the inlet system is available from the authors.

The authors of reference 44 have recently used a Knudsen cell with the same make of commercial mass spectrometer; their operational capabilities appear to be comparable with ours. Watanabe and Naito (ref. 45) have also adapted a Knudsen cell inlet system to a Mattauch-Herzog type mass spectrometer, but they have not specified the range of operational capability.

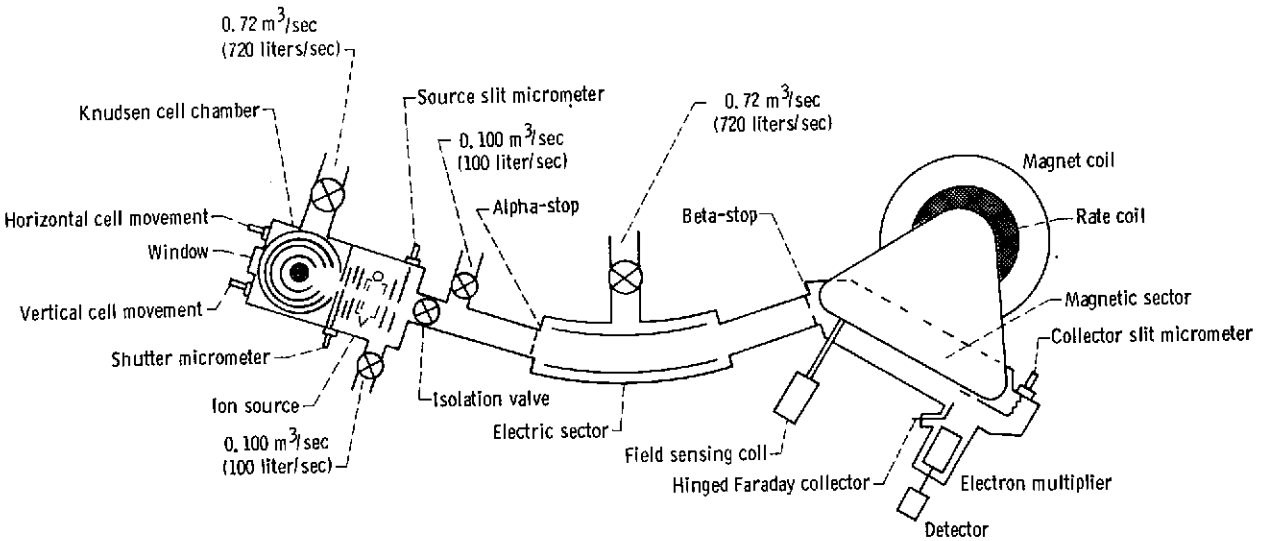

Figure 11. - Schematic of Knudsen cell inlet system and double-focusing mass spectrometer.

Knudsen Cell Inlet System

For equilibrium vaporization measurements, molecular beams are derived from a heated Knudsen cell containing the sample being investigated. The Knudsen cell is a right-circular cylinder with an effusion orifice in the side wall, three blackbody holes 180° opposite the orifice, and a close-fitting lid. A cross-sectional view of the cell is shown in figure 12. The effusion orifice is designed to have a knife edge and thus zero length to provide a Clausing factor for the orifice of close to unity. The orifice diameter is usually made less than 1 millimeter so that the ratio of the orifice area to the sample surface area is less than 0.01. Cells of this design have been fabricated with graphite, tantalum, tungsten, tantalum carbide, and hafnium carbide. Spark machining methods have been found to be most suitable to fabricate cells from the hard materials.

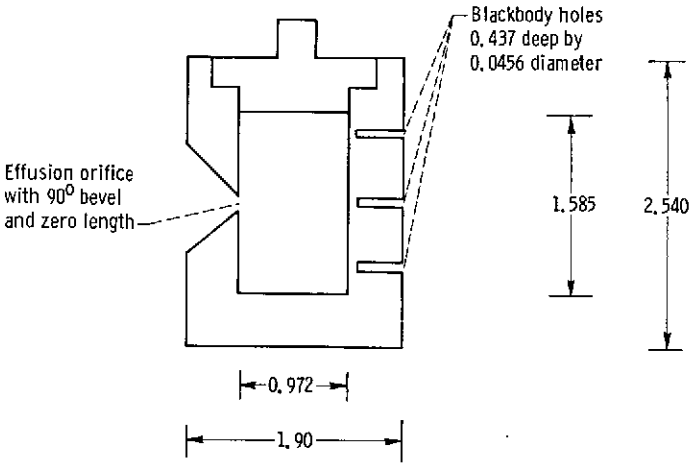

Figure 12. - Knudsen cell cross section. (Dimensions are in cm.)

The blackbody holes in the rear of the cell have a depth-to-radius ratio of 19-to-1, and this aspect ratio has been shown (ref. 46) to give an excellent blackbody approximation. We have tested this cell design by measuring temperatures with an optical pyrometer focused into the effusion orifice and into the blackbody holes. These tests demonstrated that with our heating arrangement the orifice and blackbody hole temperatures agreed within the ±3 K precision of the optical pyrometer for the temperature range from 1000 to 3300 K.

For many specific experiments it has been found necessary to fit the Knudsen cell with an appropriate liner to contain the sample. The design of the cylindrical liner is shown in cross section in figure 13. The sidewall hole in the liner is typically made one diameter larger than the effusion orifice in the Knudsen cell. The liner has its own close-fitting lid. Liners have been made of graphite, alumina, zirconia, and thoria.

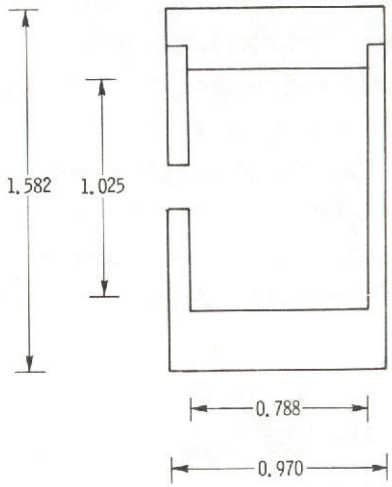

Figure 13. - Knudsen cell liner cross section. (Dimensions are in cm.)

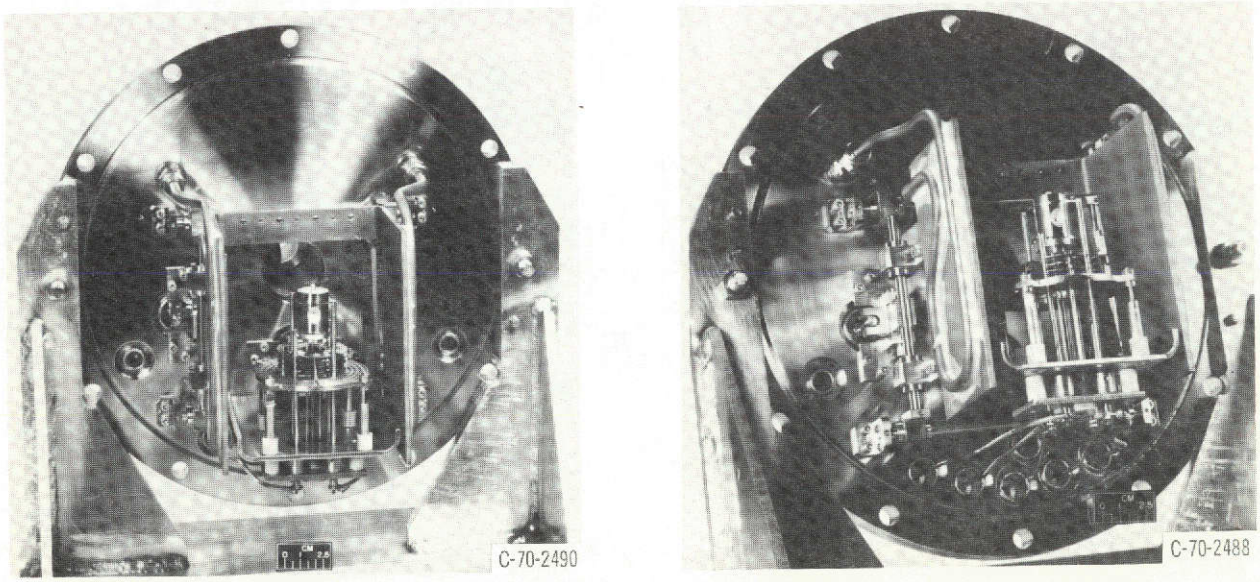

Figure 14. - Knudsen cell support system.

The Knudsen cell is supported in the oven (figs. 14 and 15) by a tantalum pedestal mounted on three tungsten rods (8 cm long, 0.125 cm diameter). The rods fit into holes in the pedestal and, at the bottom, fit into holes in a boron nitride cylinder attached to an electrically isolated base mounting plate. Threaded glazed porcelain cylinders (1.2 cm high, 1 cm diameter) provide the isolation of the base plate from the mounting fixture. A tantalum rod (1 mm diameter), protected by a ceramic tube, is screwed into the center of the pedestal. This rod passes down through a clearance hole in the boron nitride so that it can be electrically connected to the high-voltage output of the electron bombardment power supply. The Knudsen cell support has proved to be dimensionally stable at cell temperatures to 3300 K and to provide good thermal isolation.

Two tungsten filaments circumscribe the Knudsen cell and are used to heat the cell by radiation and electron bombardment. As shown in figure 14, one filament is located

1. Water-cooled shield
2. Ta heat shields
3. Knudsen cell
4. Ta filament post
5. W cell support rod
6. Ta anode
7. Porcelain insulators
8. Boron nitride support
9. Ta support plate
10. Ta mounting plate
11. Water-cooled baffle
12. Magnet pole
13. Electron filament
14. Ionization chamber
15. Electron trap
16. Shutter
17. Deflector
18. Collimator slit
19. Repeller
20. Focus plate
21. Source slit
22. Beam height aperture
23. Isolation valve

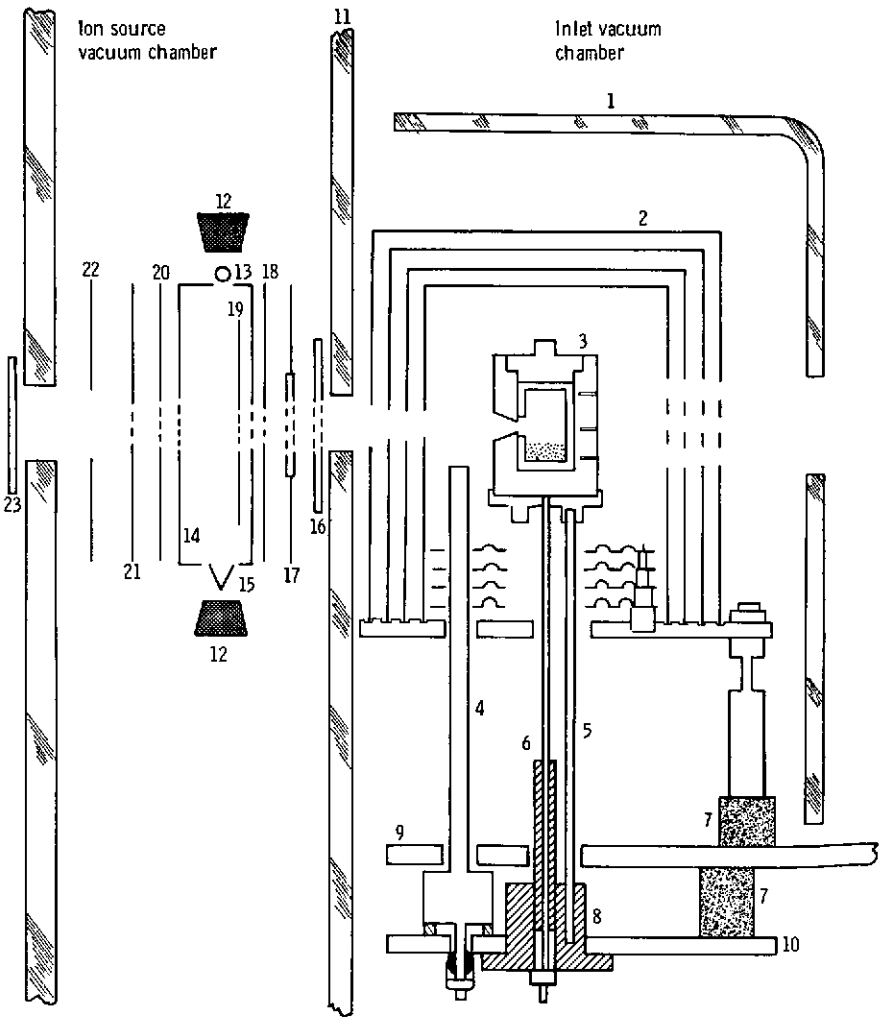

Figure 15. - Schematic of Knudsen cell over assembly and ion source.

near the top of the cell and the other is near the bottom. Each filament consists of two semicircles of 0.01- by 0.076-centimeter tungsten ribbon electrically connected in parallel. The filaments are held in place, about 0.4 centimeter from the cell, by tantalum posts (0.32 cm diameter) slotted to accept the tungsten ribbon. The filament posts are supported from the base mounting plate by ruby and zirconia insulators which provide electrical isolation.

Four tantalum heat shields (3.8 cm diameter) are located under the Knudsen cell (figs. 14 and 15). These shields are held in position by four tantalum spacers resting on a tantalum shield holder which also supports four concentric cylindrical heat shields surrounding the Knudsen cell, filaments, and lower heat shields. The heat shields (0.13 mm thick) are electrically connected to one another but isolated from ground and other parts of the system. An electrical lead connects the heat-shield assembly to ground through an ammeter in the electron bombardment power supply. The cylindrical heat shields have separate removable tops, and each shield has appropriate holes in its side to aline with the cell effusion orifice and blackbody holes. The heat shields and enclosed tungsten filaments comprise the Knudsen cell oven.

The Knudsen cell and oven assembly are secured on a tantalum fixture attached to the vacuum chamber and flange by a mechanism employing linear ball bushings. This mechanism facilitates independent horizontal and vertical translation of the cell assembly relative to the ion source entrance. Movement is controlled by manipulation of two bellows-sealed micrometers mounted on the outside of the vacuum flange. Translation range is ± 1.5 centimeters about a center position. The translation capability allows alinement of the effusion orifice with the shutter slit and ion source entrance slit.

The sides, rear, and top of the oven assembly are enclosed by a water-cooled copper heat sink, part of which can be seen in figure 14.

The Knudsen cell is heated by two modes: radiation for temperatures to about 1500 K and electron bombardment for temperatures between 1500 and 3300 K. Filament power is supplied from the 0.5 kilovolt-ampere alternating-current power source diagramed in figure 16. This circuit allows the power to each filament to be

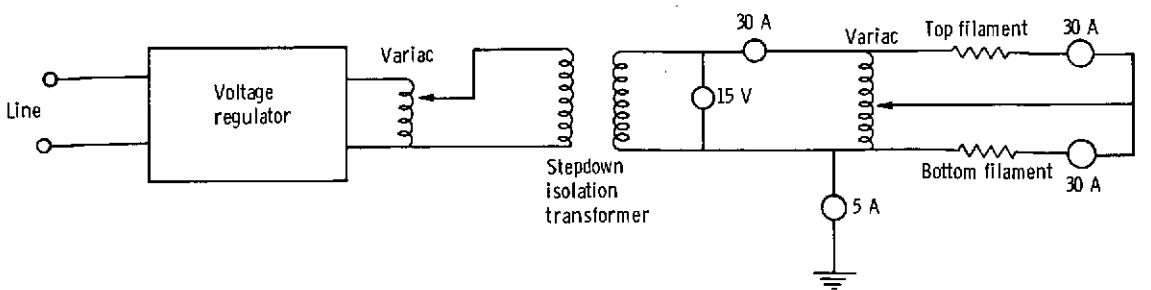

Figure 16. - Filament power circuit diagram.

proportioned so that it is possible to eliminate vertical temperature gradients in the Knudsen cell caused by differences in the filaments or their position relative to the cell. In the radiation heating mode, cell temperatures were held constant to at least ± 3 K by merely holding the power constant.

In the electron bombardment heating mode, cell temperature is achieved by control of the power fed to the oven. Figure 17 is a schematic representation of the electron bombardment power supply. The high-voltage output is connected to the Knudsen cell. The output of the high-voltage transformer passes through a series of saturable core reactors which function as a variable impedance in the line and ultimately determine the output voltage of the supply. The saturable reactor output is rectified to provide the direct-current high voltage applied to the cell. Power control is achieved by using a Hall effect transducer.

The output voltage of the Hall wafer in the transducer is directly proportional to the product of the magnetic field perpendicular to the wafer and the current flowing along the length of the wafer. The emission sense current flowing along the wafer is obtained by shunting a portion of the total emission current through resistor R_2 and the Hall wafer. The strength of the transducer magnetic field is determined by measuring the current through resistor R_5 and the magnet coil. This current is directly proportional to the output voltage of the supply. Thus, the power signal output of the Hall wafer is proportional to the product of the total emission current and supply voltage, that is, the power dissipated. This regulating system supplies as much as 5 kilowatts of power, and it regulates this power to better than 0.5 percent. In the electron bombardment mode of heating, cell temperatures of 3300 K can be attained, and temperature regulation is typically ± 5 K.

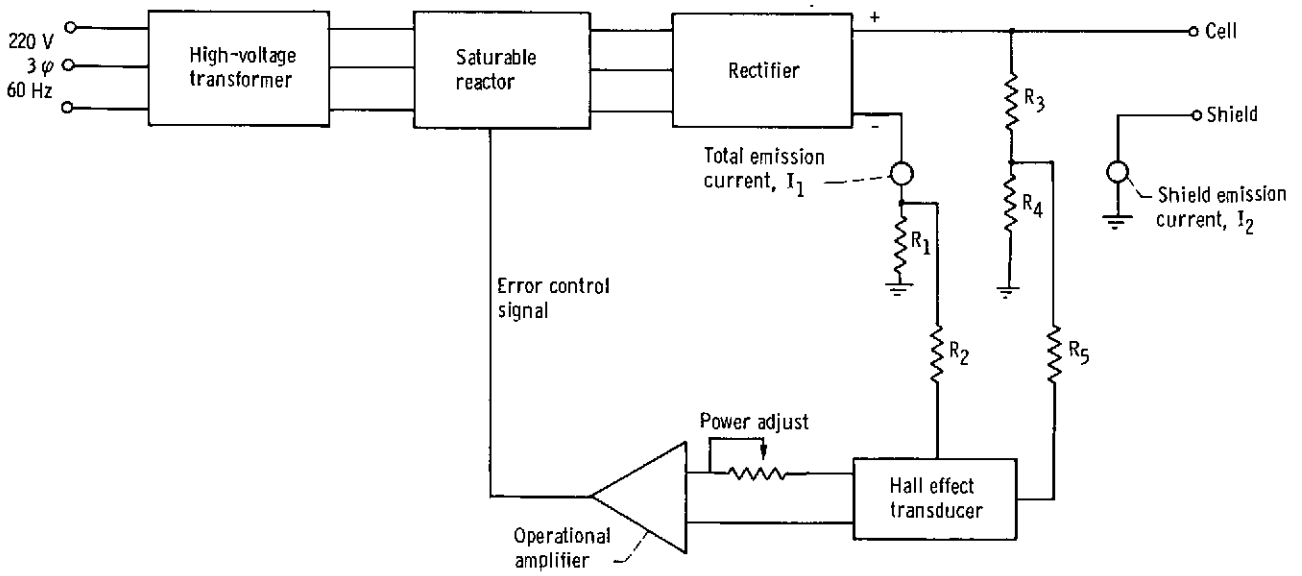

Figure 17. - Electron bombardment power supply diagram.

Knudsen cell temperatures are measured by sighting a calibrated Micro Optical brightness pyrometer into the blackbody holes in the cell. The pyrometer is sighted through an optically flat glass window mounted on the vacuum flange supporting the Knudsen cell oven. The window is protected from subliming vapors by a shutter which is magnetically actuated from outside the vacuum chamber. Experimentally determined corrections for transmission losses of the window are applied to all temperature measurements (ref. 47). By reading the temperature at each of the three blackbody holes, it is possible to detect any vertical temperature gradients in the Knudsen cell. Detected gradients are eliminated by appropriate adjustment of the ratio of power to the two filaments.

The molecular beam inlet system and ion source region of the mass spectrometer are separated by a water-cooled copper baffle which has an opening coaxial with the entrance slit of the ion source. The opening (1.0 cm by 0.6 cm) in the plate is equipped with an adjustable-width, translatable-slit shutter whose movement in the horizontal direction is controlled by a micrometer screw. By adjusting the micrometer from outside the vacuum chamber the shutter may be used to block the molecular beam, to allow optimum passage of the beam, or to scan the beam to study its profile. The width of the shutter slit is typically set at 0.5 millimeter.

High-speed pumping of the molecular beam inlet system vacuum chamber was found to be essential when working with materials that yield noncondensable vapors. Therefore, this chamber is pumped with a 0.720-m^3/sec (720 liter/sec) oil diffusion pump. A high-conductance liquid nitrogen cold trap is used above the diffusion pump to minimize back-streaming of oil vapor. Pressures in this chamber are measured with a Bayard-Alpert type ionization gage mounted on the chamber. Gold and copper gaskets are used for all vacuum seals, and the chamber can be baked out to 500 K.

Ion Source

The general features of the electron-impact-type ion source are shown schematically in figure 15. Upon entering the ion source vacuum chamber, the molecular beam passes between a pair of deflection plates and through two collimating slits before entering the chamber, where electron impact takes place. The deflector plates are separated by 0.16 centimeter, and they are used to deflect any ionic species in the molecular beam. One plate can be held at the ionization chamber potential, and the other can be set to ground potential or some fraction of the ionization chamber potential. In all our studies, no ionic species was ever detected in the molecular beam. Therefore, after testing for ionic species, both plates are set to the ionization chamber potential and held there during subsequent measurements.

The first collimating slit is 0.64 millimeter wide and floating with respect to ground. The second collimating slit is the entrance slit to the ionization chamber. It is 0.45

millimeter wide and is maintained at the ionization chamber potential of 8 kilovolts. Within the ionization chamber are a pair of isolated repeller plates whose potential can be independently varied from 0 to 200 volts relative to the chamber potential. In practice, repeller potentials of only a few volts are required to maximize the ion beam.

Electrons are produced by a heated rhenium filament (0.18 mm diameter). The shielded filament is located just outside the ionization chamber. Electrons pass from the filament through alined openings in the chamber to a gold anode (electron trap) located outside the chamber opposite the filament. The electrons passing through the chamber intersect the molecular beam at right angles. A permanent magnet around the chamber is arranged with a pole behind the filament and anode. The filament can be held at a potential of -3 to -53, -70, or -150 volts with respect to the chamber. The anode is held at 0 to 70 or 150 volts relative to the chamber. Filament emission current is electronically regulated at any selected value between 0 to 200 microamperes.

The ion beam exits from the ionization chamber through a 0.45-millimeter slit and passes through a focus slit consisting of two plates whose potential can be independently varied. The focus slit is 0.64 millimeter wide and is maintained at a potential of from 0 to -200 volts relative to the ion chamber. By varying the potential of each focus plate the ion beam is directed through the source slit and into the mass analyzer. This slit has an adjustable width of from 0 to 0.5 millimeter. The width is set by manipulation of a micrometer screw located outside the ion source vacuum chamber, and the width is set according to the resolution desired. The source slit is at ground potential.

The ion source electronics are designed to facilitate direct continuous recording of ionization efficiency curves. The ionizing voltage can be continuously varied by a variable-speed-motor-driven, 10-turn linear potentiometer incorporated into the circuit. A second 10-turn potentiometer is ganged to the first but electrically isolated from it. This second potentiometer is part of a simple direct-current circuit whose output is directly proportional to the ionizing voltage. The output of this circuit is used to feed the x-channel of an x-y recorder used to record the ionization efficiency curves. The y-channel is driven by the output of the mass analyzer detector.

The ion source vacuum chamber is pumped by a 0.1-m^3/sec (100-liter/sec) oil diffusion pump and a liquid-nitrogen cold trap. Pressure in this chamber is measured with a Bayard-Alpert type ion gage attached to the vacuum chamber. In operation the ion source vacuum chamber is always maintained at a pressure at least a factor of 10 below that of the inlet system vacuum chamber.

Mass Analyzer

The mass analyzer consists of tandem electrostatic and magnetic sectors whose geometries are arranged to yield first-order double focusing at all masses. The theoretical considerations of this Mattauch-Herzog geometry have been extensively

reviewed in the literature (ref. 48). The general arrangement and features of our system are shown in figure 11.

The beam of ions of mixed mass and velocity emerging from the source slit travels down the field-free drift tube and through the alpha-stop into the electric sector. After traversing the electric sector, where velocity focusing occurs, the ion beam is partially intercepted by the beam monitor electrodes, passes through the beta-stop and enters the magnetic sector. Here it is separated into a series of beams composed of the various mass-to-charge ratio components. Each individual component is brought to focus at the ion detector by varying the magnitude of the orthogonal electromagnetic field. The beam must pass through an adjustable-width collector slit before encountering the detector used for electric detection. The collector slit, located at the maximum radius allowed by the magnet, can be rotated, translated, and width adjusted by manipulation of micrometers located outside the analyzer vacuum chamber. The magnet is also equipped with a photoplate for photographic detection.

The electromagnet is driven by a direct-current power supply. Regulation of the field intensity is achieved with feedback signals derived from a rotating-coil Faraday induction sensor in the field and a stationary field-rate sensing coil around the magnet yoke. The rotating coil probe has an overall diameter of 0.6 centimeter. This probe extends into the magnet gap in the same plane as the ion beam. The probe is allowed to remain outside the analyzer vacuum system by being fitted into a thin-wall stainless-steel well that protrudes into the vacuum system.

The magnetic field feedback control system used in our apparatus in an O. S. Walker Company model FFC-4. This system provides a field set accuracy of 0.1 gauss, a short-term stability of 4×10^{-6}, and a long-term stability of 10^{-5}. The system has a range of field sweep rates of from 0.1 to 10 000 gauss per minute with a sweep linearity of better than 0.1 percent of the swept range. Sweep modes include single scan, repetitive sawtooth scan, and repetitive triangular scan.

By the use of standard samples which yield known mass-to-charge ratio peaks the magnetic field settings have been calibrated in terms of mass-to-charge ratio. With this system it is possible to preset any peak to be detected, and this greatly reduces the time required for measurements.

The vacuum system of the mass analyzer is separated from the ion source by an isolation valve. A 0.1-m^3/sec (100-liter/sec) oil diffusion pump and liquid-nitrogen cold trap connected to the analyzer drift tube provides differential pumping between the analyzer and ion source. The main part of the analyzer is pumped by a 0.720-m^3/sec (720-liter/sec) fusion pump and liquid-nitrogen cold trap connected to the system at the electric sector. Pressures in the analyzer are measured with a Bayard-Alpert ionization gage located at the electric sector. Under all operating conditions the pumping system maintains the analyzer pressure below 5×10^{-8} torr.

Ion Detection

Our apparatus is equipped with both photographic and electrical means of ion detection. For all our studies the electrical detection mode was used exclusively. Therefore, discussion is limited to considerations in this area of ion detection.

In the electrical detection mode, ion currents can be measured with either a Faraday cup or an electron multiplier. The Faraday cup is used for the measurement of ion currents greater than 10^{-12} ampere (6.25×10^6 ions/sec). The electron multiplier is used for ion currents below this value. The Faraday cup is hinged so that it can be positioned to intercept the ion beam by manipulation of a lever external to the vacuum system. Electrically, the Faraday cup lead is brought out of the vacuum system through a ceramic BNC vacuum feedthrough. A Cary model 31 vibrating reed electrometer connected directly to the Faraday cup is used to measure ion currents directly when the current is sufficiently large.

When the ion current is too small to be measured directly with the Faraday cup, the cup is moved out of position and the ion beam is allowed to intercept the first dynode of a 17-stage Allen-type focused electron multiplier supplied by Consolidated Electrodynamics Corporation (CEC). The potential of each copper-beryllium dynode is variable between 128 and 256 volts. The multiplier, dynode resistors, and filtering capacitors are all contained in the mass analyzer vacuum chamber. The multplier anode is brought out of the vacuum system through a separate ceramic BNC feedthrough and all other multiplier leads are brought out through shielded ceramic feedthroughs. The general multiplier arrangement is shown schematically in figure 18.

Multiplier output currents could be measured by either direct-current or pulse-counting techniques. Each of these techniques presents certain advantages for mass spectrometry applications. Therefore, the techniques and details of the apparatus are discussed separately. For the experiments described in this report, pulse counting was used only to measure the multiplier gain for the various ionic species being studied. All other experimental measurements of ion current were made by the direct-current method.

Direct-current measurements. - For direct-current measurements the preamplifier unit of a Cary model 31 vibrating reed electrometer is coupled through the vacuum feedthrough to the anode of the electron multiplier. The preamplifier is equipped with a switch which allows input resistors of 10^9, 10^8, and 10^7 ohms to be used.

The electrometer output is fed directly to a 25.4-centimeter- (10-in.-) scale strip-chart recorder. Measurements were made by slowly scanning over each peak a minimum of five times. The scan rate was set to allow an integration time of at least 10 seconds on the top of each peak. The difference between the average peak height and background was measured for each scan, and the resulting values were averaged for the number of scans made.

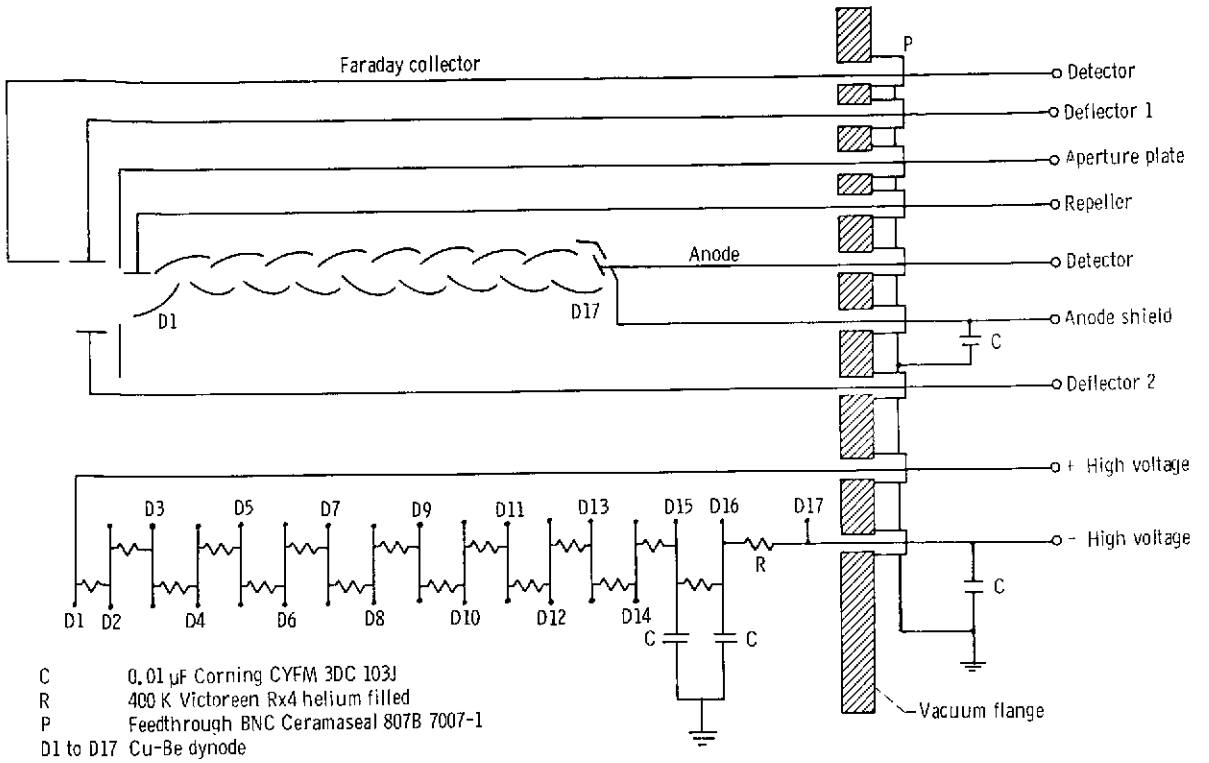

Figure 18. - Schematic of multiplier and current recording system.

In practice the minimum detectable multiplier output current signal was found to be about 10^{-12} ampere for our system of measurement. This limit is established by the noise in the electronic system, the shot noise of the multiplier, and the random nature of the signal ions being measured. To prevent a loss in gain due to local heating of the dynode surfaces, the maximum anode current was deemed to be about 10^{-6} ampere. Thus, the dynamic range of our system was 10^{6}.

Ion counting. - In principle, ion-counting techniques offer certain advantages in mass spectrometry applications (refs. 48 and 49). These advantages are (1) very low ion intensities can be measured with increased precision and accuracy; (2) electron multiplier mass discrimination effects are eliminated; (3) detrimental effects of multiplier gain instability as a function of time are minimized; (4) relative multiplier gains can be measured for ionic species whose intensities are so low that no other method is applicable; and (5) statistical analysis, data reduction, and computer interfacing are simplified. In our system we have not been able to fully realize the first advantage because of instabilities in the mass spectrometer and noise pickup in our ion-counting system electronics. Neither of these problems is insurmountable, and we have merely not made an effort to solve them.

Two different ion-counting systems have been used in our studies. The first system used allows direct-current electrometer monitoring and ion counting to be done simultaneously. The ion-counting system is coupled to the last dynode of the multiplier, while the electrometer is connected to the anode. The arrangement is shown in figure 19. Coupling to the last dynode is achieved by use of a miniature ferrite-core transformer and associated circuitry. The negative pulses are conditioned by a pulse amplifier-discriminator (Johnston Laboratories, Inc., model PAD-1) and counted by a digital counter. The multiplier and counting system were found to have a dead time of 0.8

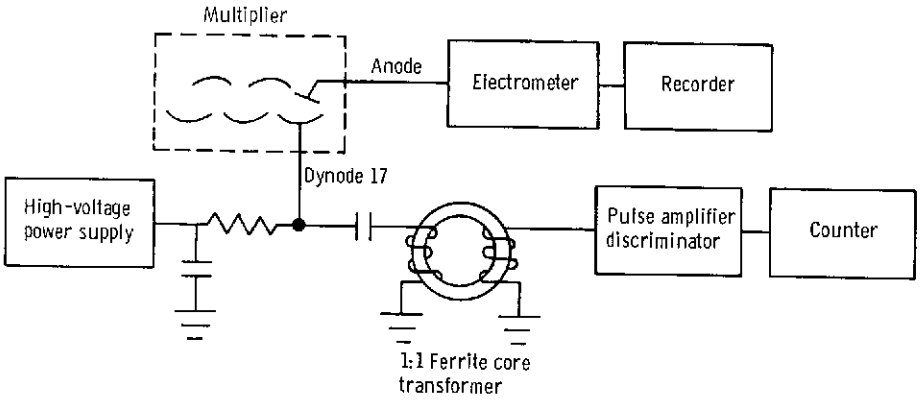

Figure 19. - Simultaneous ion counting and current recording.

microsecond. The maximum count rate of the counting system was found to be about 2×10^5 counts per second. With this counting system it was always necessary to operate the multiplier at maximum gain. Measured count rates Q were corrected for background count rate band system dead time t_λ by the expressions (ref. 50)

$$\frac{dN}{dt} = \frac{Q}{1 - Qt_\lambda} - B$$

where N is the number of ions striking the first dynode, and

$$\frac{dN}{dt} = \frac{I_e}{\gamma e^-}$$

where I_e is the current measured at the anode, γ is the multplier gain, and e^- is the charge of the electron. The background count rate B was measured for each Q by switching off the ion beam. This system was used successfully to measure the multiplier gain for ionic species, but it did not yield any increase in sensitivity over the direct-current measurement mode.

The second ion-counting system used consisted of an SSR Instrument Company model 1120 amplifier discriminator, model 1105 data converter console, and model 1110 digital synchronous computer. The low-noise, high-speed amplifier-discriminator is connected directly to the multiplier anode. In using this system with our multiplier it was necessary to shield completely all leads to the multiplier against radiofrequency pickup so as to minimize background counts. The addition of filtering capacitors to the last two dynodes of the multiplier also aided in reducing background counts. However, we have not been able to reduce the background counts to a level near the dark count rate for the multiplier, which is one count per minute at a dynode voltage of 180 volts per stage. To further improve our situation would require a redesign of our multiplier housing, and this was not deemed justifiable during our studies. A plot of total background counts versus multiplier dynode voltage is shown in figure 20.

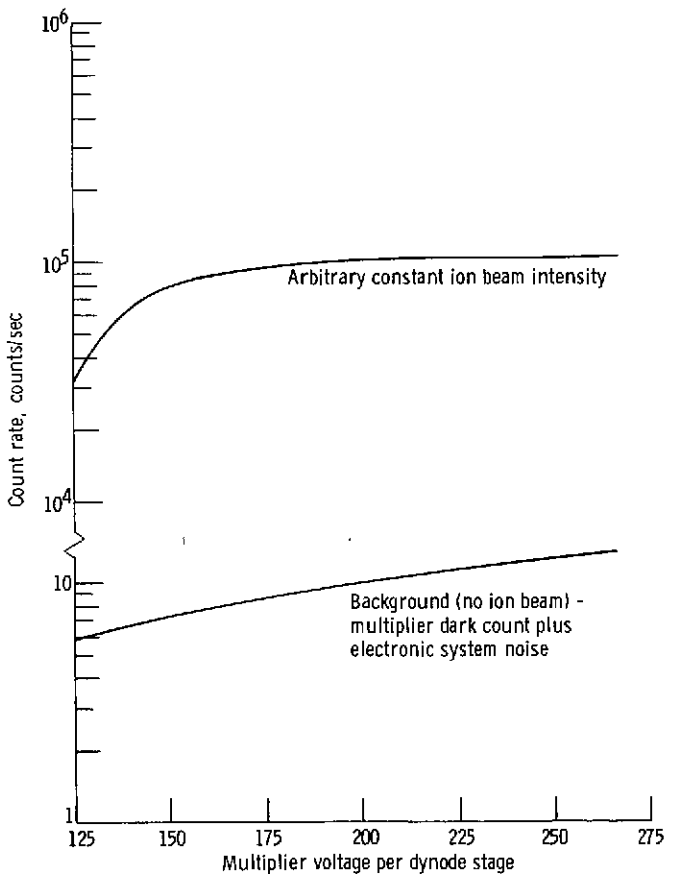

Figure 20. - Count rate as function of multiplier voltage.

The output of the amplifier-discriminator is fed to a data converter console which provides linear and logarithmic rate-meters, optional prescaling, an analog output, and a pulse output suitable for driving a high-speed pulse counter or the digital synchronous computer. Electronic details of the counting system have been adequately given by Zatzick (refs. 49 and 51, and references cited therein).

The amplifier-discriminator permits resolving electron pulses separated by as little as 10^{-8} second, and the sensitivity is sufficient for detection of pulses representing less than 10^{6} electronic charges. This high sensitivity allows operation on the "plateau" of the multiplier gain curve (ref. 49). On the plateau, alterations in count rate due to fluctuation in secondary emission characteristics of the multiplier supply voltage are reduced to negligible levels. A plateau curve for our system is shown in figure 20 for an arbitrary intensity gold peak, and the absolute gain curve for the multiplier is shown in figure 21.

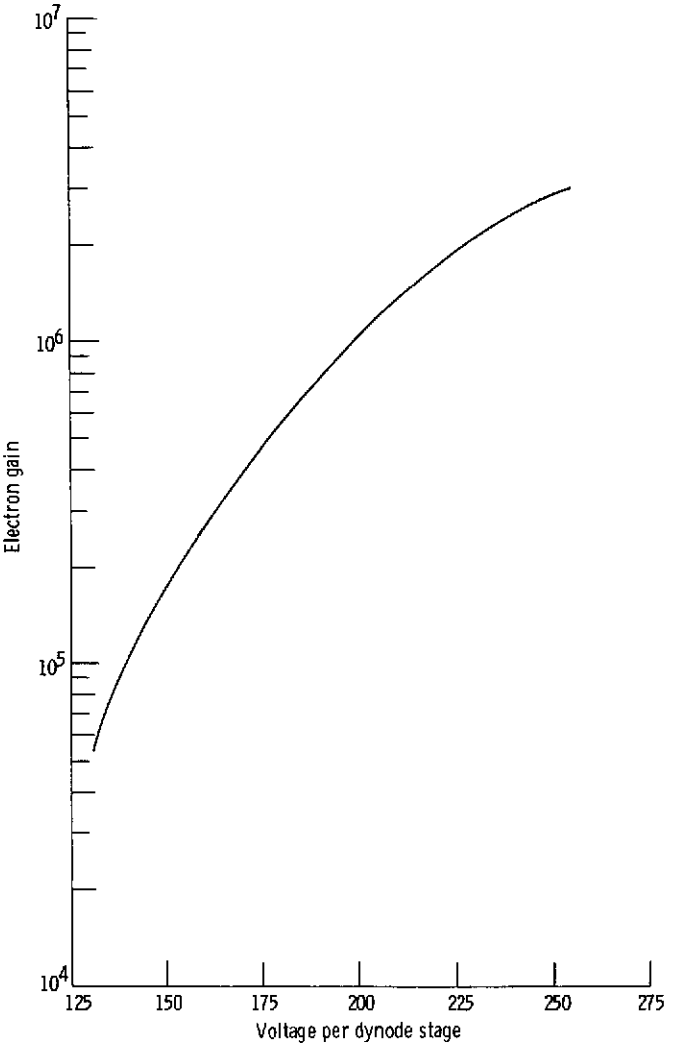

Figure 21. - Multiplier gain as a function of multiplier voltage. Multiplier, CEC 17-stage Cu-Be Allen type for Au+ ions.

Because this latter ion-counting system does not allow for simultaneous electrometer recording of peaks, it was found necessary to increase the stability of the electric sector power supply to eliminate drift from the peak maximum while counting. Increased stability was attained by adding line voltage regulation to the electric sector input and by replacing an internal voltage regulator tube with a separate, highly regulated direct-current power supply. With these modifications the stability of the total mass analyzer (electric and magnetic sectors) was quite satisfactory for ion counting.

In our studies the greatest advantage offered by ion counting is that the multiplier gain for each ionic species being studied can be measured directly. This advantage eliminates the uncertainties and other problems associated with multiplier mass discrimination (refs. 52 and 53, and references cited therein). To realize the total potential of counting techniques with our mass spectrometer, the ion transmission of the apparatus would have to be increased. Our limit of sensitivity is set by our ability to measure ion currents of about 10^{-19} ampere with a reasonable degree of accuracy. This current level corresponds to about one ion per second incident on the first multiplier dynode. At such low count rates, measurement accuracy depends to a large degree on limitations imposed by the statistics of counting random events and inherent noise properties of multipliers and electronic equipment. Signal-to-noise considerations of counting systems have been treated by a number of investigators (refs. 54 to 58).

Apparatus Performance

In the preceding descriptions of the apparatus, capabilities and evaluations of the various major components have also been presented. No single test of the entire system over its whole operating range is possible, and the reader is referred to previous publications (refs. 1, 2, 4, 5, 10, 11, and 26 to 29), which we feel demonstrate the performance of our system. Examples of high-resolution spectra and appearance potential and ionization efficiency curves are given in several of the references. In addition, we have measured the heat of vaporization of gold; the results are here presented as further evidence of the quality of our system.

A gold sample with a purity of 99.999 percent was loaded in a graphite liner in a tungsten Knudsen cell. The Knudsen cell orifice diameter was 0.75 millimeter. The cell was heated by radiation and electron bombardment. The ion source was operated with an anode current of 150 microamperes, and the energy of the ionizing electrons was 30 electron volts. The mass analyzer was operated at a resolution of 2000. Intensity of the $^{197}Au^{+}$ peak was measured as a function of temperature over the range from 1353 to 1822 K. Intensities were measured with the SSR ion counting system.

Experimental results are shown in figure 22, where the logarithm of the intensity-temperature product is plotted against reciprocal temperature. The line through the

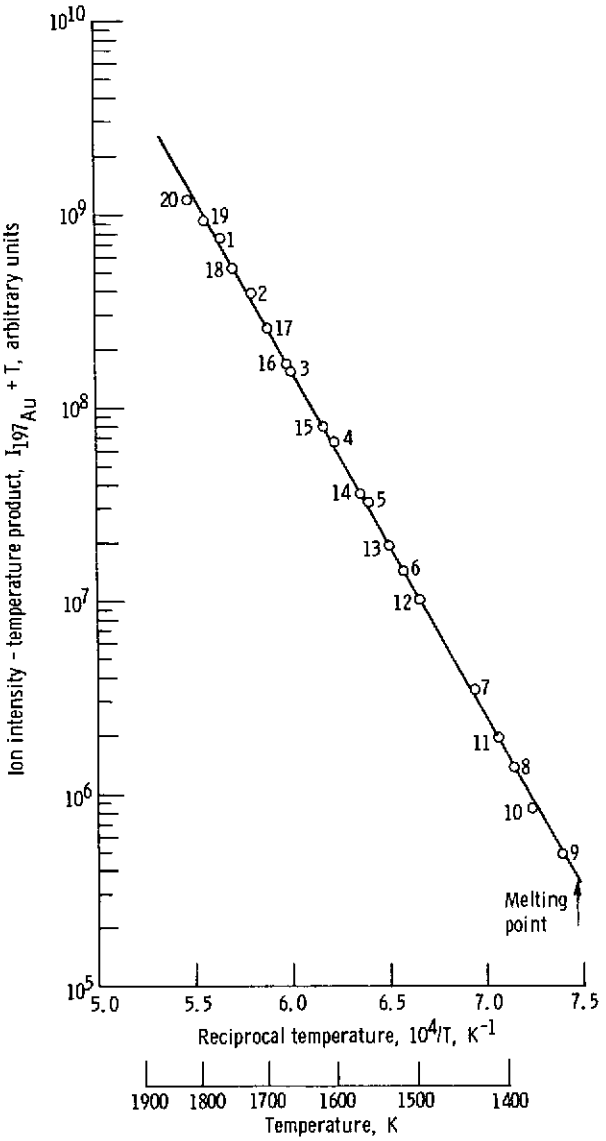

Figure 22. - Second-law heat of vaporization of gold. Au(l) = Au(g); $\Delta H^{o}_{1576\ K} = 347.1 \pm 1.9$ kJ mol^{-1}; $\Delta H^{o}_{298K} = 369.7 \pm 2.0$ kJ mol^{-1}.

data points was derived by the method of least squares, and the slope of this line yielded a second-law heat of vaporization ΔH_T of 347.1 ± 1.9 kJ mol^{-1} at the mean temperature of 1576 K. The indicated error is the standard deviation of the slope.

Conversion of ΔH_T to $\Delta H^{o}_{298\ K}$ by use of the enthalpy functions for Au(g) and Au(c) from reference 30 gives 369.7 ± 2.0 kJ mol^{-1}. This value is in excellent agreement with the selected value of 368.2 ± 1.3 kJ mol^{-1} from reference 30 and the National Bureau of Standards reference value of 367.0 ± 0.9 kJ mol^{-1} (ref. 59). The agreement demonstrates that no significant systematic errors were present for the measurement system.

REFERENCES

1. Stearns, Carl A.; and Kohl, Fred J.: The Dissociation Energies of Titanium Dicarbide and Titanium Tetracarbide. High Temp. Sci., vol. 2, no. 3, Sept., 1970, pp. 274-285.

2. Stearns, Carl A.; and Kohl, Fred J.: Mass Spectrometric Determination of the Dissociation Energies of Titanium Dicarbide and Titanium Tetracarbide, NASA TN D-5653, 1970.

3. Storms, Edmund K.: The Refractory Carbides. Academic Press, 1967.

4. Kohl, Fred J.; and Stearns, Carl A.: Dissociation Energy of Vanadium and Chromium Dicarbide and Vanadium Tetracarbide. J. Phys. Chem., vol. 74, no. 13, 1970, pp. 2714-2718.

5. Kohl, Fred J.; and Stearns, Carl A.: Mass Spectrometric Determination of the Dissociation Energy of Vanadium and Chromium Dicarbide and Vanadium Tetracarbide. NASA TN D-5719, 1970.

6. Storms, Edmund; Calkin, Brant; and Yencha, Andrew: The Vaporization Behavior of the Defect Carbides. Part I: Nb-C System. High Temp. Sci., vol. 1, no. 4, Dec. 1969, pp. 430-455.

7. Filby, E. E.; and Ames, L. L.: Dissociation Energies of the Gaseous Dicarbides of the Rare Earths. High Temp. Sci., vol. 4, no. 2, Apr. 1972, pp. 160-169.

8. Balducci, G.; De Maria, G.; and Guido, M.: Thermodynamics of the Rare-Earth – Carbon System. III. The Erbium-Carbon System. J. Chem. Phys., vol. 51, no. 7, Oct. 1, 1969, pp. 2876-2879.

9. Balducci, G.; De Maria, G.; and Guido, M.: Mass Spectrometric Determination of the Dissociation Energy of $EuC_2(g)$. J. Chem. Phys., vol. 56, no. 4, Feb. 15, 1972, pp. 1431-1433.

10. Stearns, Carl A.; and Kohl, Fred J.: Vaporization Thermodynamics of the Lanthanum Carbon System. Mass Spectrometric Determination of the Dissociation Energy of LaC_2, LaC_3, and LaC_4. J. Chem. Phys., vol. 54, no. 12, June 15, 1971, pp. 5180-5187.

11. Kohl, Fred J.; and Stearns, Carl A.: Mass Spectrometric Determination of the Dissociation Energy of ScC_2 and ScC_4. J. Chem. Phys., vol. 54, no. 3, 1971, pp. 1414-1416.

12. Kohl, Fred J.; and Stearns, Carl A.: Mass Spectrometric Knudsen Cell Studies of Vaporization of Lanthanum and Scandium Carbides and Dissociation Energy of LaC_2, LaC_3, LaC_4, ScC_2, and ScC_4. NASA TN D-7039, 1971.

13. De Maria, G.; Balducci, G.; Capalbi, A.; and Guido, M.: High Temperature Mass Spectrometric Study of the System Neodymium-Carbon. Proc. British Ceram. Soc., vol. 8, 1967, pp. 127-136.

14. Chupka, William A.; Berkowitz, Joseph; Giese, Clayton F.; and Inghram, Mark G.: Thermodynamic Studies of Some Gaseous Metallic Carbides. J. Phys. Chem., vol. 62, May, 1958, pp. 611-614.

15. Giengerich, Karl A.: Mass-Spectrometric Evidence for the Molecules UC and CeC and Predicted Stability of Diatomic Carbides of Electropositive Transition Metals. J. Chem. Phys., vol. 50, no. 5, Mar. 1, 1969, pp. 2255-2256.

16. Vander Auwera-Mahieu, A.; and Drowart, J.: The Dissociation Energies of the Molecules PtC and RhC. Chem. Phys. Letters, vol. 1, Oct. 1967, pp. 311-313.

17. McIntyre, N. S.; Vander Auwera-Mahieu, A.; and Drowart, J.; Mass Spectrometric Determination of the Dissociation Energies of Gaseous RuC, IrC, and PtB. Trans. Faraday Soc., vol. 64, 1968, pp. 3006-3010.

18. Drowart, J.; Pattoret, A.; and Smoes, S.: Mass Spectrometric Studies of the Vaporization of Refractory Compounds. Proc. British Ceram. Soc., vol. 8, 1967, pp. 67-89.

19. Cocke, D. L.; and Gingerich, K. A.: Determination of the Heats of Atomization of the Molecules RhC_2, RhC, and TiC_2 by High Temperature Mass Spectrometry. J. Chem. Phys., vol. 57, no. 9, Nov. 1, 1972, pp. 3654-3661.

20. Starostina, T. S.; Sidorov, L. N.; Akishin, P. A.; and Karasev, N. M.: Mass Spectrometric Investigation of the Composition of the Vapor Above the Systems TiC-C and ZrC-C. Izv. Akad. Nauk SSSR, Neorg. Mater., vol. 3, no. 4, 1967, pp. 647-648.

21. Torshina, V. V.; Smolina, G. N.; Dobychin, S. L.; Avarbe, R. G.; and Vilk Yu. N.: Mass-Spectrometric Study of the Vaporization of Zirconium Carbide at High Temperatures. Refractory Carbides. G. V. Samsonov, ed., Kiev, Izdatel' stvo Naukova Dumka, 1970, pp. 197-200.

22. Jackson, Donald D.; Barton, George W., Jr.; Krikorian, Oscar H.; and Newbury, Ray S.: Vaporization of Thorium Dicarbide, J. Phys. Chem., vol. 68, no. 6, June 1964, pp. 1516-1523.

23. Jackson, D. D.; Barton, G. W., Jr.; Krikorian, O. H.; and Newbury, R. S.: Vaporization of Gadolinium and Thorium Dicarbide. Thermodynamics of Nuclear Materials. International Atomic Energy Agency, Vienna, 1962, pp. 529-548.

24. Kent, R. A.: The Vaporization and Thermodynamics of Thorium Dicarbide. Ph. D. Thesis, Michigan State Univ., 1963.

25. Tsuji, T.: Molecular Abundances in Stellar Atmospheres. II. Astronomy and Astrophys., vol. 23, no. 3, 1973, pp. 411-431.

26. Stearns, Carl A.; and Kohl, Fred J.: The Dissociation Energy of Gaseous Titanium Mononitride. NASA TN D-5027, 1969.

27. Kohl, Fred J.; and Stearns, Carl A.: Mass Spectrometric Investigation of Vaporization Thermodynamics of Yttrium Dicarbide - Carbon System and Dissociation Energy of Yttrium Dicarbide and Tetracarbide. NASA TN D-5646, 1970.

28. Kohl, Fred J.; and Stearns, Carl A.: Vaporization Thermodynamics of Yttrium Dicarbide - Carbon System and Dissociation Energy of Yttrium Dicarbide and Tetracarbide. J. Chem. Phys., vol. 52, no. 12, June 15, 1970, pp. 6310-6315.

29. Stearns, Carl A.; and Kohl, Fred J.: Dissociation Energies of Some High Temperature Molecules Containing Aluminum. NASA TN D-7123, 1972.

30. Hultgren, Ralph; Orr, Raymond L.; Anderson, Philip D.; and Kelly, Kenneth K.: Selected Values of Thermodynamic Properties of Metals and Alloys. Univ. California, Dept. Mineral Tech., Supplements, issues dated Jan. 1966 for Hf(g); Feb. 1967 for Th(g); Aug. 1969 for Au(c, g); and Apr. 1968 for Ag(c, g).

31. Mann, Joseph B.: Ionization Cross Sections of the Elements Calculated from Mean-Square Radii of Atomic Orbitals. J. Chem. Phys., vol. 46, no. 5, Mar. 1, 1967, pp. 1646-1651.

32. Drowart, J.; and Goldfinger, P.: Investigation of Inorganic Systems at High Temperature by Mass Spectrometry. Angew. Chemie. Int. Ed., vol. 6, no. 7, July 1967, pp. 581-596.

33. Stull, D. R., ed.: JANAF Thermochemical Tables. Dow Chemical Co., issues dated Mar. 31, 1961 for C(s) and C(g); June 30, 1967 for Ti(g); Dec. 31, 1967 for Zr(g); and Dec. 31, 1969 for $C_2(g)$, $C_3(g)$, $C_4(g)$, and $C_5(g)$.

34. Walsh, A. D.: The Electronic Orbitals, Shapes, and Spectra of Polyatomic Molecules. Part II. Non-hydride AB_2 and BAC Molecules. J. Chem. Soc., pt. 3, 1953, pp. 2266-2288.

35. Cheetham, C. J.; and Barrow, R. F.: The Spectroscopy of Diatomic Transition Element Molecules. Advances in High Temperature Chemistry. Vol. 1. LeRoy Erying, ed., Academic Press, 1967, pp. 7-41.

36. Herschbach, Dudley R.; and Laurie, Victor W.: Anharmonic Potential Constants and Their Dependence Upon Bond Length. J. Chem. Phys., vol. 35, no. 2, 1961, pp. 458-463.

37. Herzberg, Gerhard: Infrared and Raman Spectra of Polyatomic Molecules. Vol. II of Molecular Spectra and Molecular Structure. D. Van Nostrand Co., Inc., 1945, pp. 173-174.

38. Engler, W.; and Kohlrausch, K. W. F.: The Raman Spectrum of N_3H and C_3O_2. Z. Physik Chem. (Leipzig), vol. B34, 1936, pp. 214-224.

39. Brewer, Leo; and Green, David W.: The Low-Lying Electronic States of ScF, TiO, ZrO. High Temp. Sci., vol. 1, no. 1, May 1969, pp. 26-45.

40. Brewer, Leo; and Rosenblatt, Gerd M.: Dissociation Energies and Free Energy Functions of Gaseous Monoxides. Advances in High Temperature Chemistry. Vol. II. LeRoy Erying, ed., Academic Press 1969, pp. 1-83.

41. McBride, Bonnie J.; and Gordon, Sanford: FORTRAN IV Program for Calculation of Thermodynamic Data. NASA TN D-4097, 1967.

42. Belton, G. R.; and Fruehan, R. J.: The Determination of Activities by Mass Spectrometry - Some Additional Methods. Met. Trans., vol. 2, no. 1, Jan. 1971, pp. 291-296.

43. Roboz, John: Introduction to Mass Spectrometry. Interscience Publishers, 1968, pp. 11-16.

44. Wachi, Francis M.; Gilmartin, Donald E.; and Roux, Donald A.: High-Temperature Mass Spectrometry. Vol. II. Knudsen Cell Assembly for Herzog-Mattauch Type Mass Spectrometer. Rep. TR-0200(4250-40)-6, vol. 2, Aerospace Corp. (SAMSO-TR-71-231, vol. 2, AD-732857), Sept. 15, 1971.

45. Watanabe, E.; and Naito, M.: Development of a Mass Spectrometer Equipped With Both a Convertible Knudsen Cell Ion Source and a R. F. Spark Ion Source. Recent Developments in Mass Spectroscopy. K. Ogata and T. Hayakawa, eds., University Park Press, 1970, pp. 249-256.

46. DeVos, J. C.: Evaluation of the Quality of a Blackbody. Physica, vol. 20, 1954, pp. 669-689.

47. Cater, E. D.: Measurement of the Gross Equilibrium Vaporization Rate (Knudsen Methods). Physicochemical Measurements in Metals Research. Vol. IV of Techniques of Metal Research. R. A. Rapp, ed., Interscience Publishers, 1970, pp. 80-82.

48. McDowell, Charles A., ed.: Mass Spectrometry, McGraw-Hill Book Co., Inc., 1963.

49. Zatzick, M. R.: How to Make Every Photon Count. Electro-Optical Syst. Des., June 1972, pp. 20-23, 26-27.

50. Barton, G. W., Jr.; Gibson, L. E.; and Tolman, L. F.: Ion Counting and Accumulation System for Mass Spectrometry of Very Small Samples. Anal. Chem., vol. 32, no. 12, Nov. 1960, pp. 1599-1601.

51. Zatzick, M. R.: Applying Digital Techniques to Photon Counting. Research/Development, Nov. 1970.

52. Lao, R.C.; Sander, R.; and Pottie, P. F.: Discrimination in Electron Multipliers for Atomic Ions. I. Multiplier Yields for 24 Mass-Analyzed Ions, Int. J. Mass Spectrom. Ion Phys., vol. 10, no. 3, 1973, pp. 309-313.

53. Pottie, R. F.; Cocke, D. L.; and Gingerich, K. A.: Discrimination in Electron Multipliers for Atomic Ions. II. Comparison of Yields for 60 Atoms. Int. J. Mass Spectrom. Ion Phys., vol. 11, no. 1, 1973, pp. 41-48.

54. Alfano, R. R.; and Ockman, N.: Methods of Detecting Weak Light Signals. J. Opt. Soc. Am., vol. 58, 1968, pp. 90-95.

55. Morton, G. A.: Photon Counting, Appl. Opt., vol. 7, no. 1, Jan. 1968, pp. 1-10.

56. Franklin, M. L.; Horlick, Gary; and Malmstadt, H. V.: Basic and Practical Considerations in Utilizing Photon Counting for Quantitative Spectrochemical Methods. Anal. Chem., vol. 41, no. 1, Jan. 1969, pp. 2-10.

57. Ingle, J. D., Jr.; and Crouch, S. R.: Pulse Overlap Effects on Linearity and Signal-to-Noise Ratio in Photon Counting Systems. Anal. Chem., vol. 44, no. 4, Apr. 1972, pp. 777-784.

58. Ingle, J. D., Jr.; and Crouch, S. R.: Critical Comparison of Photon Counting and Direct Current Measurement Techniques for Quantitative Spectrometric Methods. Anal. Chem., vol. 44, no. 4, Apr. 1972, pp. 785-794.

59. Paule, R. C.; and Mandel, J.: Standard Reference Material 745, Gold Vapor Pressure. National Bureau of Standards, 1969.

60. Kiser, Robert W.: Introduction to Mass Spectrometry and Its Applications. Prentice-Hall, Inc., 1965, app. IV.

61. Herzberg, Gerhard: Spectra of Diatomic Molecules. Vol. I of Molecular Spectra and Molecular Structure. Second ed., D. Van Nostrand Co., Inc., 1950, app.

62. Storms, E. K.: A Mass Spectrometric Study of the Vapour Pressure of U(g) and UC_2(g) Over Various Compositions in the Uranium-Carbon System. Thermodynamics. Vol. 1. International Atomic Energy Agency, Vienna, 1966, pp. 309-343.